





Design, development, and control of a tough electrohydraulic hexapod robot for subsea operations

I. Davliakos, I. Roditis, K. Lika, Ch.-M. Breki & E. Papadopoulos


To cite this article: I. Davliakos, I. Roditis, K. Lika, Ch.-M. Breki & E. Papadopoulos (2018): Design, development, and control of a tough electrohydraulic hexapod robot for subsea operations, *Advanced Robotics*, DOI: [10.1080/01691864.2018.1461684](https://doi.org/10.1080/01691864.2018.1461684)

To link to this article: <https://doi.org/10.1080/01691864.2018.1461684>

 View supplementary material [↗](#)

 Published online: 03 May 2018.

 Submit your article to this journal [↗](#)

 Article views: 63

 View related articles [↗](#)

 View Crossmark data [↗](#)

Design, development, and control of a tough electrohydraulic hexapod robot for subsea operations

I. Davliakos^a, I. Roditis^b, K. Lika^a, Ch.-M. Breki^b and E. Papadopoulos^a

^aSchool of Mechanical Engineering, National Technical University of Athens, Athens, Greece; ^bInnora SA, Koropi, Greece

ABSTRACT

In this paper, the design, the development, and the control for an 18 degree-of-freedom electrohydraulic hexapod robot for subsea operations are presented. The hexapod, called HexaTerra, can be equipped with a trenching machine, and move over obstacles and on sloped terrain. Optimization techniques are employed to size the robot legs. Rigid body equations of motion and hydraulic dynamics are developed. Compact electrohydraulic components are sized and selected taking into account the leg kinematics and system dynamic analysis. A model-based control system design is implemented in a real-time environment, able to produce the overall functionality and performance. Experimental results obtained from preliminary tests with the developed electrohydraulic hexapod show good controlled performance and demonstrate excellent system stability over obstacles.

ARTICLE HISTORY

Received 31 July 2017
Revised 8 February 2018
and 30 March 2018
Accepted 2 April 2018

KEYWORDS

Hexapod robot;
electrohydraulic mobile
robot; underwater
hydraulics; model-based
hydraulic control; hexapod
stability and control

1. Introduction

Hydraulics science combined with automatic control has given new thrust to hydraulics applications. The main reasons why hydraulics are preferred to electromechanical drives in a number of industrial and mobile applications include their ability to produce large forces at high speeds, their high durability and stiffness, and their rapid response [1,2]. Hydraulic regimes differ from electromechanical ones, in that the force or torque output is not proportional to actuator current and therefore, hydraulic actuators cannot be modeled as force/torque sources, but rather as variable impedances.

Underwater robots are employed in a number of scientific, exploration, commercial, and military tasks. Underwater robots include Remotely Operated Vehicles (ROVs) or Autonomous Underwater Vehicles (AUVs). Although these can be used in underwater repairs and exploration, they cannot be used in tasks on the seabed or shores, such as laying cables. Legged, tracked, or even wheeled underwater robots can be used as subsea explorers or navigators and for operations such as trenching. However, underwater tracked and wheeled vehicles cannot operate over rough, sloped, or discontinuous terrain, as they can become unstable easily [3]. Because of their ability to lift their legs over obstacles, place them in a

range of discontinuous stance points, and change the main body position and attitude by adjusting leg configuration, subsea legged robots can be more stable than other types of robots, rejecting environmental disturbances from sea currents, slopes, etc.

Large hexapod robots carrying large payloads usually are driven hydraulically because of the high torque/force to weight ratio of hydraulic actuators. Further, its high static stability margin enables them dexterous at hazardous environments. Also, the hydraulic actuators normally remain at the last position when the pump is accidentally stopped or the control valve is failed. This actually provides a locking capability of the actuators, and the robot is saved from collapse. Therefore, hydraulically actuated hexapod robots with many independently actuated joints are rendered as the most suitable systems for walking or running robot applications.

Early work associated with the design and control of legged robots has employed electrohydraulic servoactuators [4]. Boston Dynamics' BigDog, built in 2005, was powered by a one-cylinder gas engine driving through a hydraulic pump its four legs. Each of them had four hydraulic actuators including a hydraulic cylinder, a valve, a position sensor, and a force feedback sensor [5–7]. The ITT 12-DOF hydraulic quadruped HyQ has been developed to perform highly dynamic tasks like jumping and

running [8]. A newer version of the HyQ, called HyQ2Max, added new skills such as a self-righting capability, and is more rugged and powerful, compared to its predecessor [9]. A hybrid control architecture for a hexapod platform, called Weaver hexapod, which enables a legged robot to autonomously traverse uneven terrain and to adapt the gait parameters depending on the terrain characteristics was developed [10]. The robot's autonomy was achieved using visual-inertial odometry on a custom built hardware setup. The LAURON V, an electrically actuated six-legged robot that accommodates 4 DOFs per leg and can be used for complex mobile manipulation tasks, is described in [11]. Its kinematics allows agile motion on rough terrain and manipulation of objects using the front legs. Although these robots were built for tough environments, these do not include the underwater ones, as special design requirements have to be met for these. Sang-Ho Hyon, et al. presented the design of a hydraulically actuated leg, aiming to agile legged locomotion [12]. The leg uses lightweight links combined with linear hydraulic actuators and its performance is evaluated using hydraulic servo actuator dynamics in a number of different control scenarios.

A mechanism design optimization algorithm of a hydraulic-actuated quadruped robot was developed in order to implement the ability of carrying heavy loads and adapting to rough dry terrains [13]. The algorithm was based on the kinematics and dynamics equations of robot, and the design parameters were optimized, using a particle swarm optimization algorithm. A design of a quadruped robot configuration driven by linear hydraulic servo cylinders with 12 active joints has been studied to plan the foot trajectory composed of cubic polynomial [14,15]. A hexapod walking forest harvester machine prototype has been developed, in 1995, by Plustech Ltd, Finland, (a John Deere Corp. subsidiary). The walking machine has been designed so that the legs spread the weight of the main body evenly, minimizing soil erosion and damage to tree roots [16]. A trajectory tracking controller of a hydraulically driven hexapod robot has been developed using an adaptive fuzzy algorithm [17]. The adaptation law of the feedback controller has been designed based on Lyapunov synthesis and its adaptation rate was varied by fuzzy self-tuning. A water hydraulic manipulator, called TEKES WHMAN, was optimized as a case study for a given manipulator requirement specification in order to illustrate and verify developed comprehensive design guidelines and performance metrics [18]. This research raised the need for design guidelines and performance metrics for comparison and improvement of different manipulators versus task requirements.

All the above robots were designed for dry terrain operation; in contrast, few legged robots for underwater operations have been built. An electromechanical, DC motor-actuated underwater six-legged walking robot named

AQUAROBOT was developed for underwater inspection for port construction [19]. An electromechanically driven underwater hexapod robot, called the Crabster CR200, is a seabed walking robot, developed and tested for shipwreck inspection and seafloor tomography surveys down to 200 meters [20]. The six-leg CR200 is equipped with six optical cameras on each side of the main body for visual inspection around the main body. The maximum power of the robot is 20 kW and the maximum walking speed is 0.5 m/s.

Hydraulic actuation systems include essential off-the-shelf components such as hydraulic pumps, electric motors, accumulators, oil tanks, filters, manifolds, hydraulic hoses, and more. These components are heavy and bulky, making a hydraulic robot heavy and bulky also. Therefore, the leg mechanisms must be constructed to be tough and rather large in size to be able to support the robot main body and impart motion on it. An advantage of size is that the robot can overcome big obstacles and disturbances in rough terrain during its work cycle. Additional considerations, such as stability and speed, dictate the kinematic design of the legs and their size compared to the size of the main robot body [3].

In this paper, the design, development, and control of the HexaTerra, [21,22], electrohydraulic underwater hexapod robot for operations in an environment with severe external forces, see Figure 1, are presented. The robot has three degrees of freedom per leg, and can be equipped with a trenching machine for burying offshore wind park cables in rocky shores.

When such a robot carries a trenching machine, its motion is restricted to straight and curved paths. Without a trencher, the robot can be used for underwater exploration and additional motion modes are desirable. The robot legs are optimized taking into account task requirements and constraints. Dynamic models are developed that describe the rigid body equations of motion including its

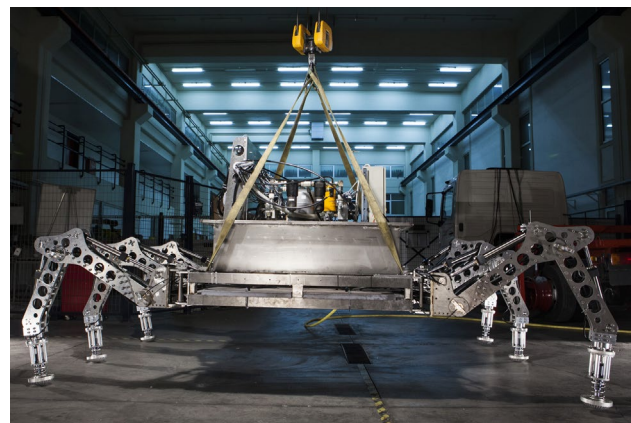


Figure 1. The hydraulically driven underwater hexapod HexaTerra, under testing at the Control Systems Lab of NTUA.

hydraulic actuation. The electrohydraulic components are selected taking into account compactness, leg kinematics, and system dynamic, aiming at size minimization, with a special emphasis in appropriate control valve selection. A model-based feedforward controller is developed in a real-time environment, able to produce the overall functionality and performance. Experimental results show good performance of the controlled hexapod and demonstrate stability over discontinuous obstacles.

2. Hexapod requirements and system modeling

2.1. Initial considerations

A large number of wind turbines are installed in windy off-shore areas. The power they produce must be transferred to the land by underwater cables, buried in the bottom of the sea. The task of laying the power cables is undertaken by heavy-duty underwater trenching machines, carried by tracked underwater vehicles. However, tracked vehicles cannot transverse steep and rocky subsea shores plagued with underwater currents, as they are subject to tipping over risks. To avoid these risks, no trenches are constructed over such shores, but the power cables are simply laid over the rocks, resulting in cable damages, breakages, and subsequent high costs for the power utilities.

One way to address this challenge is to use trenching machines on legged vehicles that can locomote over rocky cliffs, and overcome the toughness and currents of the subsea environment. As trenching speeds are slow, while static stability is of paramount importance, the simplest statically stable legged machine, i.e. a hexapod, emerges as the best choice.

To explore the possibility of using underwater hexapods in trenching and exploration tasks on rocky shores, a scaled-down hexapod was designed, built, and tested. Its specifications were obtained from those of a future full-scale machine according to scaling rules. Following the opposite path, the scaled-down design will be scaled up to result in the full-scale hexapod. This paper describes the modeling, design, development, and control of the scaled-down underwater electrohydraulic hexapod.

Among the specifications, perhaps the most difficult to satisfy were (a) the requirement that the hexapod should operate both subsea and outside the water at slopes overcoming obstacles of various geometries, (b) to carry a substantial payload, i.e. the trencher, during trenching tasks, and (c) to maintain stability in the presence of large trenching forces and torques, underwater currents, and gravitational pulls on slopes. The need to satisfy these requirements in a tough underwater environment made this field hexapod robot an innovative engineering achievement. Some of the specifications for the scaled-down hexapod are given below:

- Robot main body dimensions not to exceed – 2.4 L × 1.2 W × 0.7 H m.
- Leg dimensions allowing to overcome obstacles of 0.5 H × 0.3 L m.
- Slopes of 20° and 15° along the longitudinal and transverse axes, respectively.
- Max system dry weight with payload – not to exceed 2000 kg.
- Forward speed of 0.05 m/s.

The geometry of the hexapod and the dynamic analysis precedes the selection of the hydraulic components. This analysis can provide the hexapod worst-case condition, which in turn can be used to size the robot and its electrohydraulic actuation.

Although the hexapod can move in a number of gaits (tripod, tetrapod, and pentapod), it is straightforward to see that the worst case occurs when it moves in a tripod gait during which three of its legs are in swing (tripod swing phase), while the other three are in contact with the ground (tripod stance phase). The worst case also includes motion on a sloped terrain of pitch (20°) and roll (15°) slopes, full load (2000 kg), and application of trenching forces (800 N) and current forces (400 N) applied in a direction opposite to its motion. A constant robot linear velocity $v = 0.05$ m/s is assumed. This worst-case scenario is used in the leg design, presented in Section 3.

Another point, which must be addressed before the leg detailed design, is the DOFs per leg. As the hexapod main body must be able to control its distance from the ground, while moving on a plane parallel to it, and at the same time its attitude must be controllable, the main body of the hexapod must possess six DOFs. To this end, its mobility is calculated using the Chebyshev–Grübler–Kutzbach criterion. We study two cases. In the first all legs are down, and in the second three legs are down and three swing. When all legs are down, and assuming three links per leg, the total number of bodies $n = 20$ ($6 \times 3 + 1 + 1$), the number of single DOF joints is $j_1 = 18$ (6×3), and the number of spherical joints corresponding to the toes on the ground is $j_3 = 6$ (6×1). Therefore, the mobility m is found to be,

$$\begin{aligned} m &= 6(n - 1) - 5j_1 - 4j_2 - 3j_3 - 2j_4 - j_5 \\ &= 6 \times (20 - 1) - 5 \times 18 - 3 \times 6 = 6 \end{aligned} \quad (1)$$

When three legs are swinging, then the mobility is,

$$\begin{aligned} m &= 6(n - 1) - 5j_1 - 4j_2 - 3j_3 - 2j_4 - j_5 \\ &= 6 \times (11 - 1) - 5 \times 9 - 3 \times 3 = 6 \end{aligned} \quad (2)$$

It can be shown that the mobility is also six during the tetrapod and pentapod gaits; therefore, three DOFs per leg is an appropriate choice. An RRR linkage representing the kinematic structure of the hexapod's leg is shown in Figure 2.

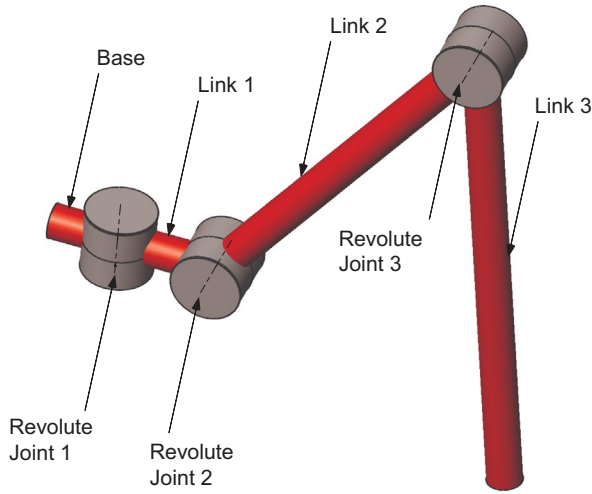


Figure 2. Basic kinematic structure of the leg.

2.2. Rigid body dynamics

To design the hexapod and its electrohydraulic actuation system, a rigid body model is needed. To this end, it is assumed that all joints are actuated with torques applied on them directly, and that the link masses are concentrated at the link Center of Mass (COM). The position, velocity, and acceleration of the links comprising the model are expressed with respect to a fixed inertial coordinate system.

Since no apriori information about the ground morphology is available, to fully define the position of all legs and the main body, the following 24 variables are chosen as generalized coordinates \mathbf{q} : (a) three coordinates describing the position vector of the main body COM with reference to the inertial system, (b) three coordinates describing the main body attitude (Euler ZYX angles) and (c) $3 \times 6 = 18$ coordinates describing the rotational DOFs of the legs. Of those, only 18 are directly actuated.

The dynamical equations describing the robotic mechanism can be calculated according to the Euler-Lagrange formulation to result in the following equation,

$$\mathbf{M}(\mathbf{q}) \ddot{\mathbf{q}} + \mathbf{V}(\mathbf{q}, \dot{\mathbf{q}}) + \mathbf{G}(\mathbf{q}) + \mathbf{T} = \mathbf{Q} \quad (3)$$

where \mathbf{M} is the mass matrix, \mathbf{V} represents forces/ torques arising from centrifugal and Coriolis forces, \mathbf{G} is a vector of gravity-induced torques, \mathbf{Q} is the vector of the generalized forces, i.e. a function of the 18 actuator-induced joint torques, of the contact forces at the toes of the legs, and \mathbf{T} is the vector of external and disturbance forces which include (a) the reaction from the ground at each leg, (b) buoyancy, (c) water resistance (drag), and (d) trenching force. The trenching force was modeled as a force proportional to robot velocity, with maximum force appearing at the maximum system velocity v . Further, a constant force (such as Coulomb friction) $\mathbf{F}_{t0} \text{sign}(v)$, and a zero-mean white noise, \mathbf{F}_{wn} , were added resulting in the following trenching force,

$$\mathbf{F}_t = b_1 v + \mathbf{F}_{t0} \text{sign}(v) + \mathbf{F}_{wn} \quad (4)$$

where b_1 is a damping coefficient. The water resisting the motion of robot was modeled as a damping force equal to $-b_2 v^2$ or $-b_2 v$ (b_2 is a damping coefficient), depending on whether the flow is turbulent or laminar, correspondingly. The buoyancy was obtained by calculating the total volume of the robot.

To study the interaction of the hexapod with the ground, it is necessary to use an appropriate model describing the behavior of the ground. To this end, a simple mass-spring-damper system is employed, see Figure 3.

2.3. Electrohydraulic actuation dynamics

Due to the tough underwater conditions and the large mass of underwater vehicles, their actuation is always electrohydraulic. Therefore, the scaled-down version of the full-scale hexapod also had to have electrohydraulic actuation, even if electric actuation could have been an alternative, see Figure 4.

The robot hydraulic system includes a hydraulic power unit and an actuation system, which consists of proportional valves, hydraulic actuators (cylinders), and hoses. The hydraulic power unit includes a three-phase electric motor, a hydraulic pump, a hydraulic accumulator, an oil tank, an oil cooler, pressure regulators for safety, relief and auxiliary valves, a manifold, hydraulic filters, and hoses. Three cylinders actuate each of the six legs at the base, shoulder, and knee DOFs, and are controlled by proportional valves, see Figure 4(b).

An ideal single rod hydraulic cylinder is described by,

$$\begin{aligned} Q_{L,p1} &= A_1 \dot{x}_p = A_1 v_p \\ Q_{L,p2} &= A_2 \dot{x}_p = A_2 v_p \\ p_{L,p1} A_1 - p_{L,p2} A_2 &= F_p \end{aligned} \quad (5)$$

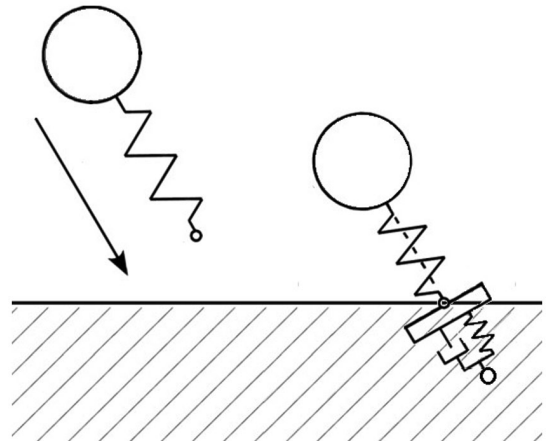


Figure 3. The ground modeled as a mass-spring-damper system, acting during contact.

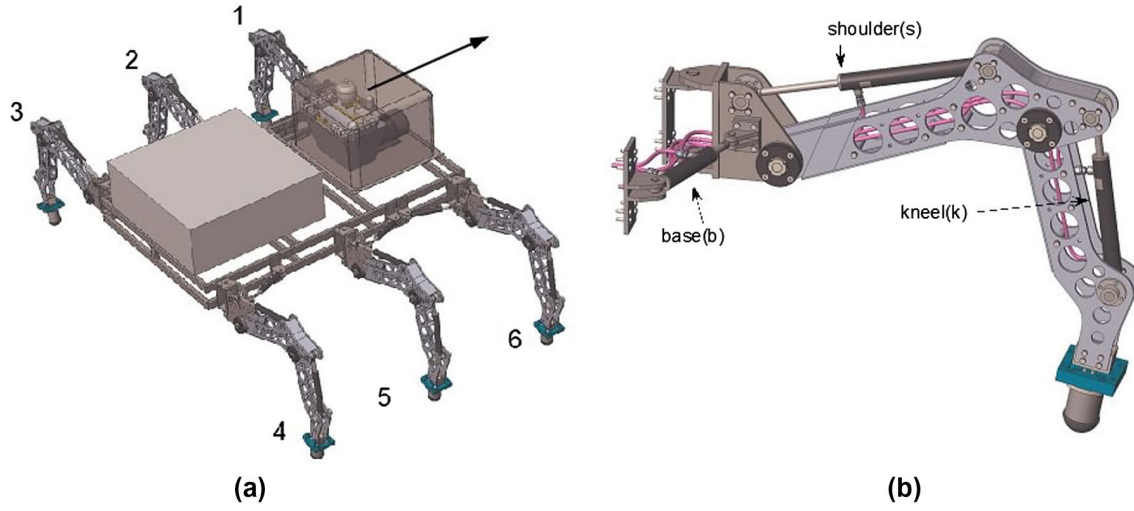


Figure 4. Hexapod electrohydraulics. (a) Full view showing the power supply, (b) a leg.

where $Q_{L,p1}$, $Q_{L,p2}$ are the flows through its two chamber ports, $p_{L,p1}$, $p_{L,p2}$ are the cylinder chamber pressures, A_1 is the piston side area, A_2 is the rod side area, x_p is the piston displacement, and F_p is the piston output force. A real cylinder model also includes chamber oil compressibility, friction, and other effects. However, these can be neglected at an initial stage.

Control of hydraulic systems is achieved through the use of control valves. Only the valve resistive effect is considered here since their bandwidth is much higher than frequencies in the controlled system. Assumed valve ideal geometry, the valve elemental (orifice) equations for the two symmetrical orifices is, [23,24],

$$\Delta p_{v,i} = KQ_{v,i}|Q_{v,i}|, \quad i = 1, 2 \quad (6)$$

where $\Delta p_{v,i}$ is the valve pressure drop at each valve orifice, $Q_{v,i}$ is the corresponding flow through an orifice, and K is a coefficient, which depends on the orifice area S , the discharge coefficient C_d and the mass density of the fluid ρ ,

$$K = 0.5\rho C_d^{-2}S^{-2} \quad (7)$$

In general, the K is a function of the *Reynolds* number and valve geometry, when the orifice flow is turbulent. However, it can be approximated by a constant [2].

Hydraulic power units regulate and supply the required hydraulic power of the servo plant. Hydraulic pumps for servo applications are piston pumps, modeled as constant pressure sources supplying power P given by,

$$P = p_s Q_s \quad (8)$$

where p_s is the constant pump pressure and Q_s is the pump supplied flow. Most of this power is dissipated at the control valves, and the rest mainly by the mechanical load and then by the hoses and auxiliary valves of the system.

Neglecting secondary effects [25], a simple pressure compatibility equation yields,

$$p_s = \Delta p_v + |\Delta p_L| \quad (9)$$

where Δp_v is the control valve pressure drop, given by Equation (6), and Δp_L is the pressure drop across the cylinder, given by,

$$\Delta p_L = p_{L,1} - p_{L,2} \quad (10)$$

where $p_{L,1}$ and $p_{L,2}$ are the two chamber pressures of the cylinder.

A hydraulic system includes hydraulic accumulators for filtering pump pressure pulsations, and for allowing the use of smaller rating pumps, by providing additional flow when needed. An accumulator, modeled as a hydraulic capacitor, is described by,

$$Q_c = C_f \frac{dp_c}{dt} \quad (11)$$

where Q_c is the fluid flow to the accumulator, p_c is the accumulator pressure, and C_f is its hydraulic capacitance.

3. Mechanical and electrohydraulic design

3.1. Leg mechanical design

The hexapod main body and its legs must be able to overcome obstacles. As shown in Figure 5, three kinds of obstacles depending on their size are identified and named as the *ridge*, the *bench*, and the *shelf*. The ridge corresponds to a tall and narrow obstacle. The shelf, to a very long obstacle compared to the length of the hexapod. The bench corresponds to an obstacle of an intermediate size. It is desired that the robot is designed such that its legs can overcome the ridge and the bench keeping the

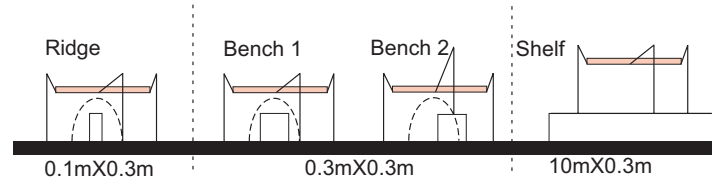


Figure 5. Ridge, bench, and shelf obstacles.

main body distance from the ground constant, in just one leg gait, even if this can be done with two gaits (bench 2 in Figure 5). These requirements call for a leg link length optimization procedure.

3.1.1. Optimization of leg lengths

As shown in Figure 6, when overcoming an obstacle, three critical foot positions emerge. The first, (1), is the starting point, the second, (2), is the middle of the trajectory where the toe is above a bench obstacle, and the third, (3), is the end of the trajectory.

The toe is considered as the end effector of a manipulator mounted at point 0 on the hexapod main body, see Figure 6. Then, the toe position with respect to 0 is given by

$${}^0\mathbf{r}_E = \begin{bmatrix} {}^0x_E \\ {}^0y_E \\ {}^0z_E \end{bmatrix} = \begin{bmatrix} \cos(q_1) \cdot (l_1 + l_2 \cdot \cos(q_2) + l_3 \cdot \cos(q_2 + q_3)) \\ \sin(q_1) \cdot (l_1 + l_2 \cdot \cos(q_2) + l_3 \cdot \cos(q_2 + q_3)) \\ l_2 \cdot \sin(q_2) + l_3 \cdot \sin(q_2 + q_3) \end{bmatrix} \quad (12)$$

where l_1, l_2, l_3 are the lengths of the links and q_1, q_2, q_3 are the angular displacements. Then, when the toe is at points (1), (2) and (3), its location is given by

$${}^0\mathbf{r}_{E,1} = \begin{bmatrix} {}^0x_{E,1} \\ {}^0y_{E,1} \\ {}^0z_{E,1} \end{bmatrix} \quad {}^0\mathbf{r}_{E,2} = \begin{bmatrix} {}^0x_{E,2} \\ {}^0y_{E,2} \\ {}^0z_{E,2} \end{bmatrix} \quad {}^0\mathbf{r}_{E,3} = \begin{bmatrix} {}^0x_{E,3} \\ {}^0y_{E,3} \\ {}^0z_{E,3} \end{bmatrix} \quad (13)$$

A foot trajectory must be selected to overcome obstacles as shown in Figure 7. The path has three straight line segments, with two curved segments of radii r , selected as a percentage of the vertical displacement of the foot, defined by the positive constant a_2 ,

$$r = a_2 z_{\max} \quad (14)$$

$$z_{\max} = {}^0z_{E,2} - {}^0z_{E,1}$$

Overcoming the obstacle in the z direction requires that

$$z_{\max} \geq s \cdot A_1 \Rightarrow s \cdot A_1 - {}^0z_{E,2} + {}^0z_{E,1} \leq 0 \quad (15)$$

where A_1 is the bench height, and s is a safety coefficient referring to the gap between the toe and the obstacle.

Overcoming the obstacle in the x direction, see Figure 7, also requires sufficient clearance, i.e.

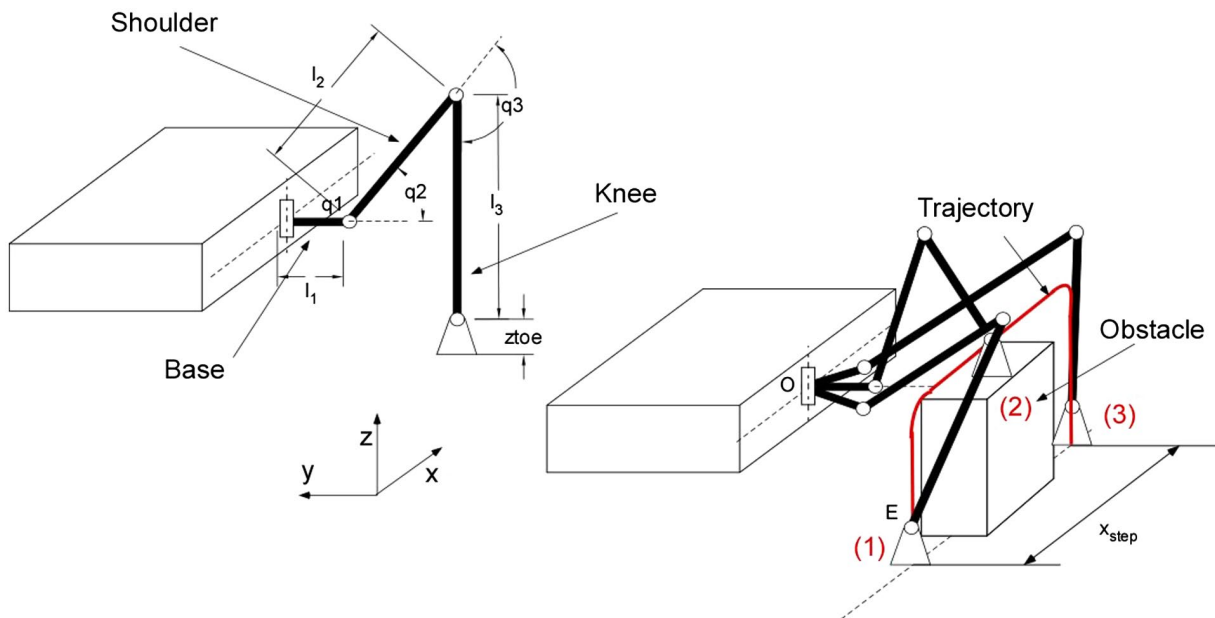


Figure 6. Three-dimensional sketch of the obstacle avoidance problem.

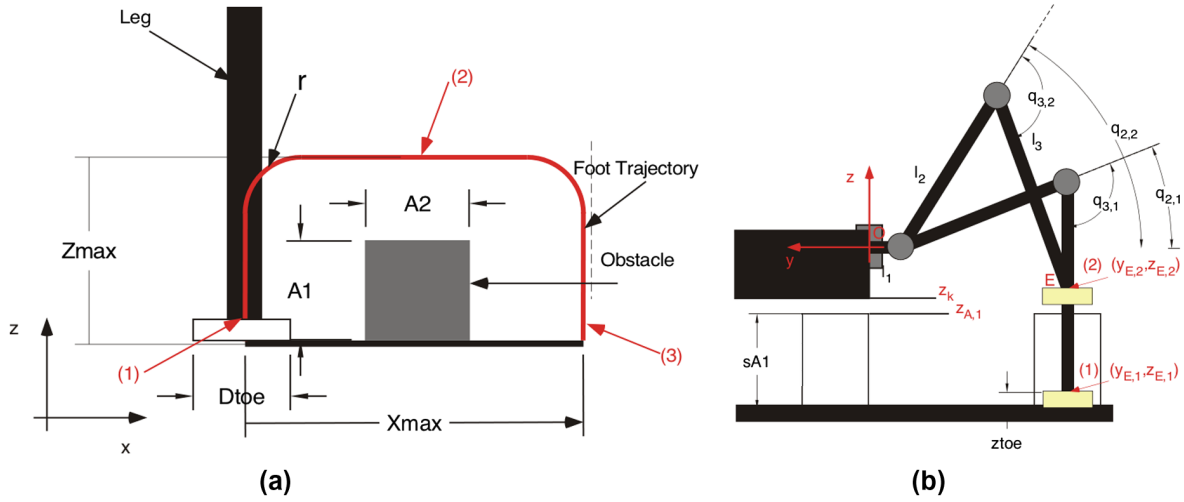


Figure 7. (a) XZ plane foot trajectory. (b) YZ plane of the foot trajectory.

$$\begin{aligned} x_{\max} = {}^0x_{E,3} - {}^0x_{E,1} &\geq A_2 + D_{\text{toe}} + 2r \Rightarrow \\ A_2 + D_{\text{toe}} + 2a_2({}^0z_{E,2} - {}^0z_{E,1}) - {}^0x_{E,3} + {}^0x_{E,1} &\leq 0 \end{aligned} \quad (16)$$

where A_2 is the bench width, and D_{toe} the diameter of the toe, modeled as a cylinder.

Since position (2) is defined as the middle of the trajectory, the following constraint must hold

$$A_2 + D_{\text{toe}} + 2 \cdot a_2 \cdot ({}^0z_{E,2} - {}^0z_{E,1}) - {}^0x_{E,2} + {}^0x_{E,1} = 0 \quad (17)$$

Not only the toe needs to overcome the obstacle, but also the main body. Therefore, according to Figure 7(b), is obtained

$$\begin{aligned} z_k \geq z_{A,1} = {}^0z_{E,1} - {}^0z_{\text{toe}} + sA_1 &\Rightarrow \\ {}^0z_{E,1} - z_{\text{toe}} + s \cdot A_1 - z_k &\leq 0 \end{aligned} \quad (18)$$

Further, the toe must move in parallel to the main body in the x direction. This will happen if

$$\begin{aligned} {}^0y_{E,1} - {}^0y_{E,2} &= 0 \\ {}^0y_{E,1} - {}^0y_{E,3} &= 0 \end{aligned} \quad (19)$$

Also, after overcoming the obstacle, the toe is asked to land at the same height as the initial one, and therefore

$${}^0z_{E,3} - {}^0z_{E,1} = 0 \quad (20)$$

Hexapod stability depends on leg opening along the y direction, see Figure 8. For the same distance of point 2 from the toe location along the y axis, and same actuation, two possible solutions exist as shown in Figure 8. Of those, the one in Figure 8(a) is preferable as it corresponds to a robot with smaller mass and volume.

The problem of leg length selection is now casted as an optimization problem. The objective function Q selected is the following

$$\begin{aligned} Q = w_1 \frac{{}^0x_{E,3}^2 + {}^0y_{E,3}^2}{l_{\max}^2} + w_2 \frac{(q_{1,3} - q_{1,1})^2}{q_{1,\max}^2} + w_3 \frac{(q_{2,2} - q_{2,1})^2}{q_{2,\max}^2} \\ + w_4 \frac{(q_{3,2} - q_{3,1})^2}{q_{3,\max}^2} + w_5 \frac{(z_{E,1} - z_{\text{toe}} + sA_1 + z_k)^2}{(sA_1)^2} \\ + w_6 \left(\left(\frac{l_1}{l_{1,\max}} \right)^2 + \left(\frac{l_2}{l_{2,\max}} \right)^2 + \left(\frac{l_3}{l_{3,\max}} \right)^2 \right) \end{aligned} \quad (21)$$

where l_{\max} , $q_{i,\max}$, $l_{i,\max}$ ($i = 1, 2, 3$), and sA_1 are normalization factors. The terms w_i , $i = 1, \dots, 6$ are weighting factors chosen such that emphasis is given to torque and leg length minimization rather than to the total angular joint displacement. In the right-hand side of Equation (21), the first term is a function of the normalized distance of the foot from the main body; this term needs to be minimized to keep the joint torques relatively small. The next three terms correspond to the normalized angular displacements during the swing phase of the first, second and third joints respectively, as defined in Figure 7(b); these need to be kept small to simplify the mechanical joint design and keep the flow rate small. The fifth term is the normalized distance (clearance) of the main body from the obstacle; this must not be excessive due to stability and joint limit reasons. The sixth term contains the link lengths l_i , $i = 1, 2, 3$ that define the total leg length and indirectly the total weight; these should be kept small. To this end, we set $w_i = 5$ ($i = 1, 5, 6$) and $w_j = 1$ ($j = 2, 3, 4$). The constraints for the optimization include

- Nonlinear inequalities and equalities as they were defined by Equations (15)–(20),

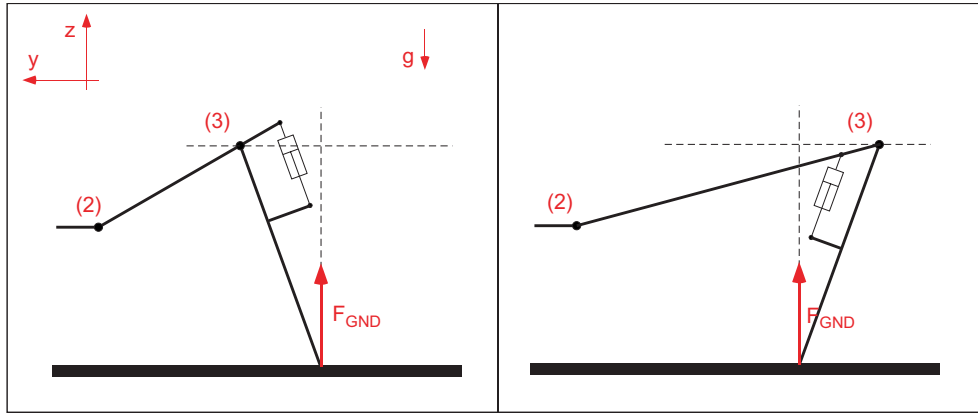


Figure 8. Alternative leg configurations for the same stability and joint torques.

- Bounds for the design variables: Lower Bound (LoB) and Upper Bound (UpB),
- A starting point (SP) for the design vector, from which the optimization starts searching for solutions.

The optimization code was developed in Matlab, using the Matlab Optimization Toolbox function `fmincon()`. The SP is the initial design vector corresponding to a solution near the optimal. It is important that this vector is chosen correctly; else the algorithm may not converge or may lead to unfeasible solutions. To obtain the necessary bounds and the SP, a rough estimation of critical parameters of the system is obtained first. The initial design vectors and design parameters are taken as $[w_1, w_2, w_3, w_4, w_5, w_6] = [1, 1, 1, 5, 5, 5]$, $[l_{\max}, l_{1,\max}, l_{2,\max}, l_{3,\max}] = [1.2 \text{ m}, 0.1 \text{ m}, 1.2 \text{ m}, 1.3 \text{ m}]$, $z_k = 0.05 \text{ m}$, $z_{\text{toe}} = 0.05 \text{ m}$, $D_{\text{toe}} = 0.1 \text{ m}$, $A_1 = 0.3 \text{ m}$, $A_2 = 0.3 \text{ m}$, $q_{i,\max} = \pi/6 \text{ rad}$ ($i = 1, 2, 3$). Table 1 displays the LoB, UpB, the SP used, as well as the optimal values of the design parameters. The computed link lengths are next used in placing the hydraulic cylinders.

3.1.2. Cylinder placement optimization in each joint

The base cylinder offsets a_1 , a_2 , and a_3 , see Figure 9, are found using the objective of minimizing piston stroke, and therefore of the power required for a given toe motion.

For technical reasons, such as collision avoidance between parts, the optimization algorithm is run several times followed by a detailed design to obtain a solution. The iterations between the optimization and detailed design yield the optimal values as $a_1 = 0.101 \text{ m}$,

$a_2 = 0.118 \text{ m}$, and $a_3 = 0.423 \text{ m}$. Using these values and the angular displacements of the main body ($\pm 20^\circ$ with respect to the horizontal, see Figure 7), the maximum and minimum cylinder lengths, and the stroke are obtained as $L_{\max} = 0.396 \text{ m}$, $L_{\min} = 0.298 \text{ m}$, and $L_{\max} - L_{\min} = 0.098 \text{ m}$, respectively. The optimization employs a detailed scalar set of component databases, which include real industrial data related to key hydraulic components, such as the cylinder overhead and¹ piston diameter.

Next, the stroke minimization of the *shoulder* and *knee* cylinders is considered. The same constraint equations and inequalities are used for both. For the leg to be able to fold completely for storage reasons, q_2 must be able to reach 90° with respect to the horizontal, and q_3 must approach 180° . The actuators must be able to apply maximum torque at joints 2 and 3 during nominal operation corresponding to the ranges in Table 1, when reaction forces are applied to the toe. The rest is similar to the main body case.

The design parameters to be optimized are shown in Figure 10, in the form of simplified sketches based on Figure 9.

The optimization constraints include:

- Singularities avoidance. Since the horizontal is at 90° ($9\pi/18$), using the axes in Figure 10, and the range for φ_1 is $\pm 20^\circ$ ($\pm 2\pi/18$) with respect to the horizontal, singularities must not occur for $\varphi_1 = 9\pi/18 \pm 2\pi/18$, or for $9\pi/18 \leq \varphi_1 \leq 11\pi/18$.
- Cylinder overhead. When retracted, the cylinders must have at least the geometrical offset (0.173 m) provided by the manufacturer. Thus,

Table 1. Optimization parameters and the optimal values for the design parameters.

	l_1	l_2	l_3	$q_{2,1}$	$q_{3,1}$	$q_{1,1}$	$q_{2,2}$	$q_{3,2}$	$q_{1,3}$	$q_{2,3}$	$q_{3,3}$
LoB	0.1	0.3	0.4	$\pi/18$	$-\pi$	$-\pi$	0	$-\pi$	$-\pi/2$	0	$-\pi$
UpB	0.2	1	1.2	$\pi/3$	$-\pi/4$	$-\pi/2$	$\pi/2$	$-\pi/4$	0	$\pi/4$	$-\pi/4$
SP	0.1	0.9	0.75	0.042π	-0.55π	-0.57π	$\pi/4$	-0.67π	-0.43π	0.042π	-0.55π
Optimal values	0.213	0.63	0.69	$\pi/18$	-0.45π	-0.59π	-0.31π	-0.58π	-0.41π	$\pi/18$	-0.45π

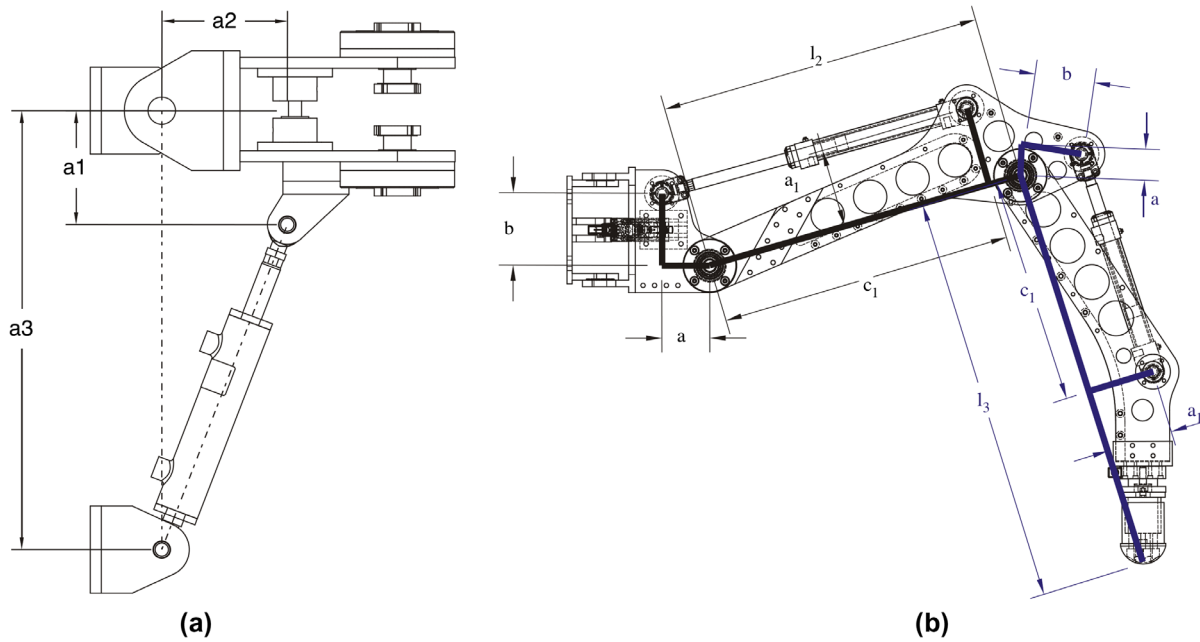


Figure 9. Hydraulic cylinder optimization parameters. (a) Base, (b) Shoulder, and Knee.

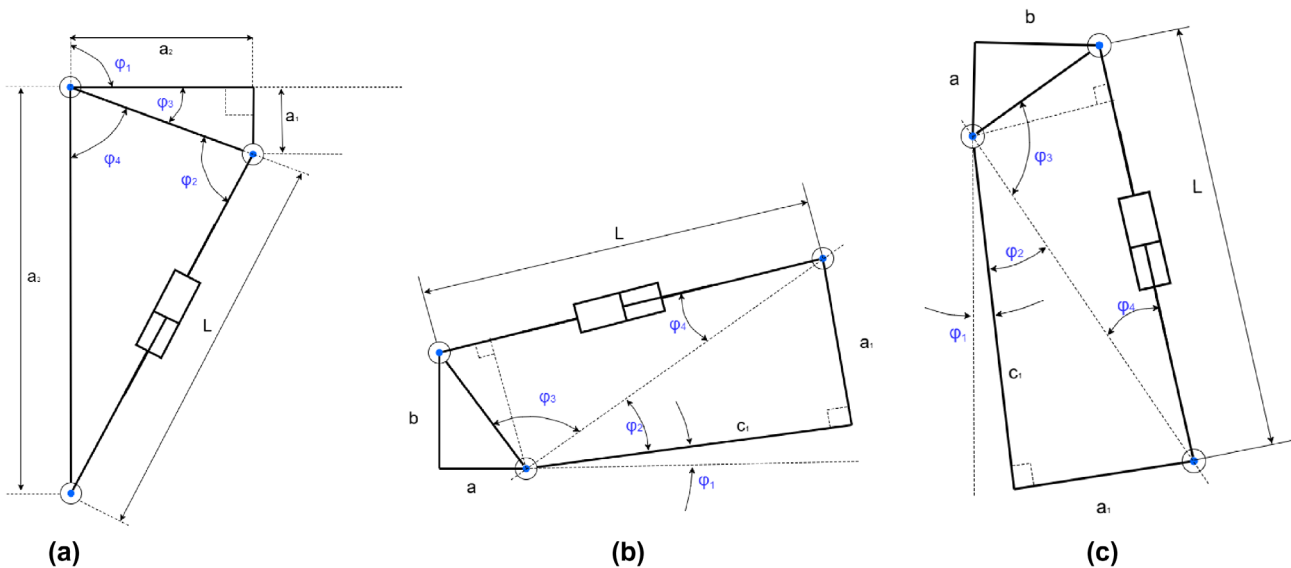


Figure 10. (a) Base, (b) shoulder, and (c) knee cylinder optimization parameters.

the stroke must be increased by the overhead. In more detail, the cylinder stroke (max. extension) $L_{\min} - L_{\text{offset}} = L_{\min} - 0.173$ must be larger than the stroke required by the trajectory, $L_{\max} - L_{\min}$; therefore, $L_{\max} - 2L_{\min} + 0.173 \leq 0$.

(c) Given the maximum cylinder thrust, and maximum load torque applied, a minimum leverage to produce the torque should exist.

The objective functions and constraints employed are defined in Table 2, for each DOF.

Table 3 displays the full optimization results, obtained using `fmincon()`, where subscript s corresponds to the shoulder, and k to the knee. For the shoulder cylinder, the procedure yields $L_{\max} = 0.659$ m, $L_{\min} = 0.430$ m, $Stroke = 0.229$ m, and for the knee, $L_{\max} = 0.579$ m, $L_{\min} = 0.389$ m, and $Stroke = 0.190$ m.

3.2. Electrohydraulic actuation

The electrohydraulic actuation system is designed based on the worst case as described earlier, i.e. during tripod

Table 2. Objective functions and nonlinear inequalities for the base, shoulder, and knee optimization.

	Base	Shoulder	Knee
<i>Objective function</i>	$Q = \frac{(L_{\max} - L_{\min})^2}{L_{\max}^2}$	$Q = \frac{(L_{\max} - L_{\min})^2}{L_{\max}^2}$	$Q = \frac{(L_{\max} - L_{\min})^2}{L_{\max}^2}$
<i>Constraints</i>			
(a)	$\frac{170}{180}\pi + \varphi_4 + \varphi_2 \leq 0$ ($\varphi_1 = 7\pi/18, 11\pi/18$)	$a \tan\left(\frac{b}{a}\right) - a \tan\left(\frac{c_1}{a_1}\right) + \frac{10}{180}\pi \leq 0$	$a \tan\left(\frac{b}{a}\right) - a \tan\left(\frac{c_1}{a_1}\right) + \frac{10}{180}\pi \leq 0$
(b)	$L_{\max} - 2L_{\min} + 0.173 \leq 0$	$L_{\max} - 2L_{\min} + 0.173 \leq 0$	$L_{\max} - 2L_{\min} + 0.173 \leq 0$
(c)	$0.060 - \cos(\varphi_4) \sqrt{a_2^2 + a_1^2} \leq 0,$ ($\varphi_1 = \frac{\pi}{18}$)	$0.120 - \sin(\varphi_4) \sqrt{c_1^2 + a_1^2} \leq 0,$ ($\varphi_1 = \frac{\pi}{18}$)	$0.120 - \sin(\varphi_4) \sqrt{c_1^2 + a_1^2} \leq 0,$ ($\varphi_1 = \frac{8\pi}{18}$)

Table 3. Optimal values for base, shoulder, and knee design parameters.

Parameter	a_1	a_2	a_3	a_5	b_5	$a_{1,s}$	$c_{1,s}$	a_k	b_k	$a_{1,k}$	$c_{1,k}$
Optimal values	0.101	0.118	0.423	0.093	0.141	0.155	0.566	0.111	0.059	0.110	0.448

Table 4. Basic kinematic and dynamic properties for the hexapod legs.

Legs 1, ..., 6	$l_{b,i} = 0.128$ m	$l_{s,i} = 0.63$ m	$l_{k,i} = 0.69$ m
----------------	---------------------	--------------------	--------------------

gait motion on sloped terrain, and with external forces from currents and trenching. The robot legs and actuators are labeled in Figure 5, while the basic robot parameters are presented in Table 4. The obstacle dimensions are taken as before to be $A_1 = 0.5$ m and $A_2 = 0.3$ m, see Figure 7(a). The $m_{b,i}$, $m_{s,i}$, and $m_{k,i}$, $i = 1, 2, \dots, 6$, are the leg link masses, which correspond to the base, shoulder, and knee cylinder for leg i , respectively ($i = 1, 2, \dots, 6$), and $l_{b,i}$, $l_{s,i}$ and $l_{k,i}$ are the link lengths which correspond to the base, shoulder, and knee, respectively ($i = 1, 2, \dots, 6$).

Using the worst-case tripod gait scenario, and the properties in Table 4, the angular velocities of the base, shoulder, and knee joints for the three legs in contact with the ground, 1, 2, and 3, are presented in Figure 11.

In Figure 11, the angular velocities' subscripts bi , si , and ki stand for the base, shoulder, and knee joint, respectively, for leg i ($i = 1, 2, 3$). Notice that the results for legs 1 and 3 coincide, as both legs are on the same side of the hexapod.

Using the system dimensions, the joint rates, and the inverse dynamics of the robot, the force, velocity, and power requirements for all robot cylinders are computed and the results, for e.g. for leg 1, are presented in Figure 12. Specifically, the inverse dynamics provide the required joint torques, which are then mapped to required cylinder forces through simple nonlinear geometric equations. In a similar way, the joint rates are mapped to cylinder velocities. The required mechanical power from the cylinders is

obtained as the product of forces and velocities. The results are obtained for the robot moving on a sloped ground of 20° toward the directional axis and 15° along an axis normal to it; therefore, the loads for this motion are not symmetrical. For sizing the cylinders, the worst loading in any leg is used.

The cylinder lengths and strokes found in Section 3.1 were used. The cylinder and cylinder rod diameters were selected for a nominal pressure of 160 bar. Using the forces, velocities, and power histories, the maximum forces, velocities, and required power for each cylinder were computed. As the maximum force for each cylinder is calculated, all cylinder diameters can be selected from commercial catalogs. All cylinders were mounted on leg links, and therefore they were selected to be waterproof. One of the cylinders is shown in Figure 13.

The electrohydraulic components of HexaTerra hydraulic power unit were sized taking into account the leg kinematics. The design of the hydraulic power unit was designed to be symmetric and as compact as possible. Thus, two identical hydraulic sub-circuits per three legs were introduced, each of which included nine control valves, a nine-valve manifold, an accumulator, and a pressure filter.

Using the worst-case scenario for hexapod motion, and using cylinder velocities and Equation (5), the flow requirements were calculated and shown in Figure 14. Since the system pressure is constant, the variations in flow are also variations in hydraulic power. The maximum hydraulic power required can be reduced significantly, resulting in a smaller pump and electric motor, if

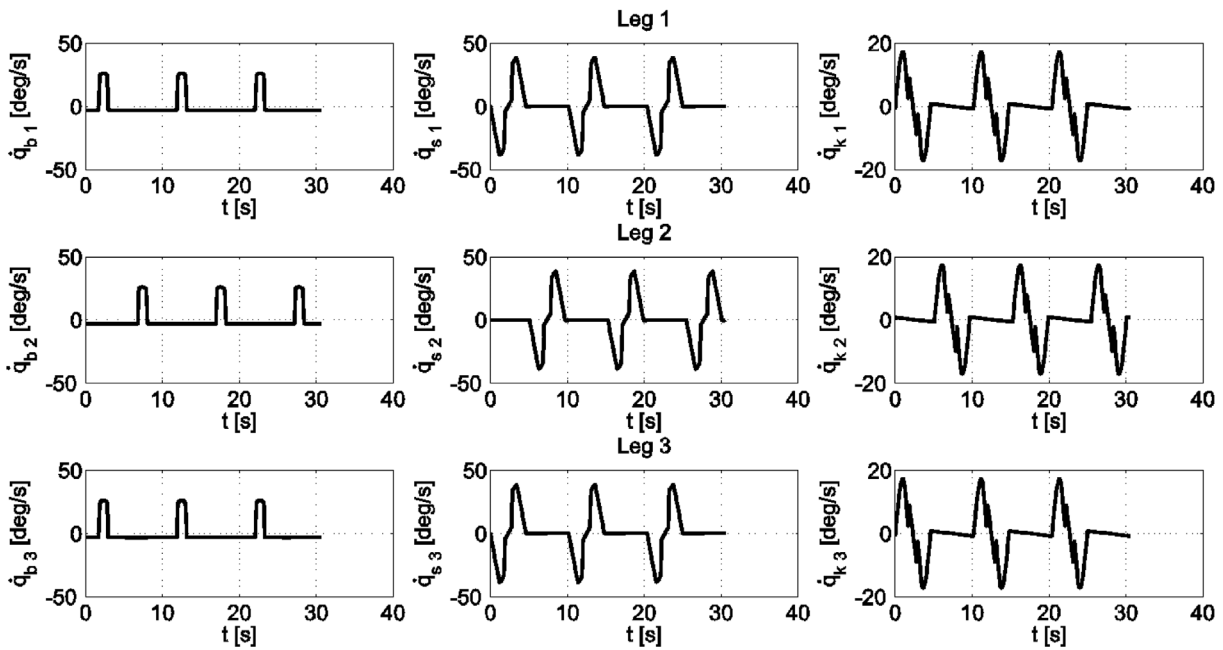


Figure 11. Angular velocities of base, shoulder, and knee joints for legs 1, 2, 3, for the worst-case scenario.

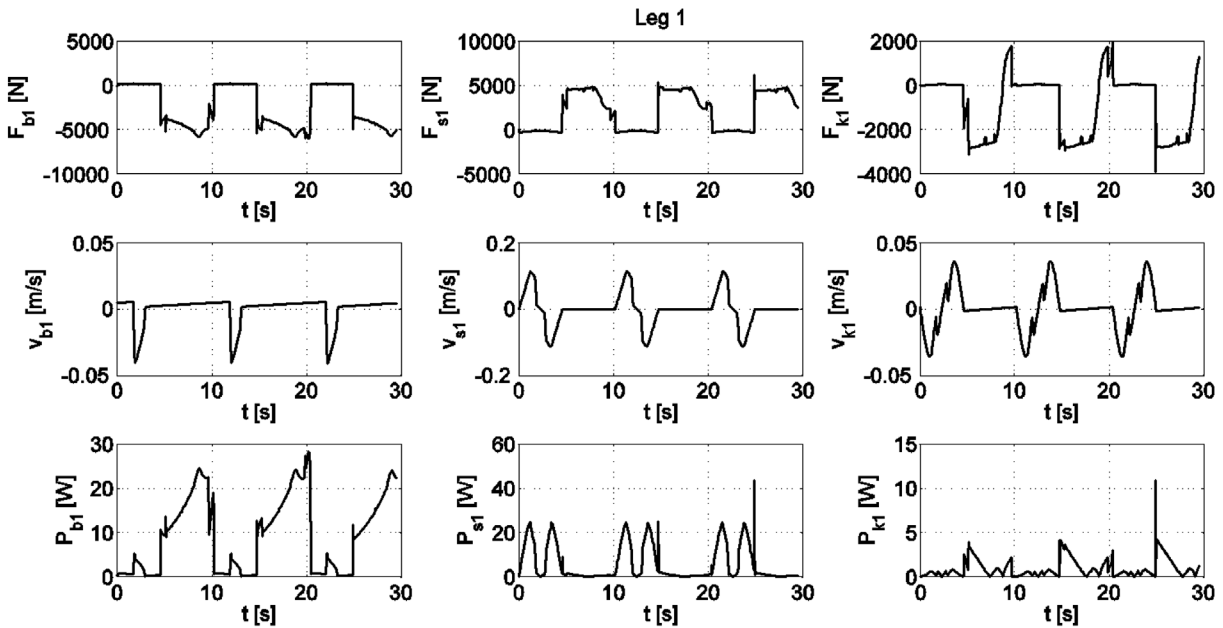


Figure 12. Leg 1 forces, velocities, and power for base (b), shoulder (s), and knee (k) cylinders.

an accumulator is added to the power supply. In the presence of an accumulator, the pump flow can be averaged to 6.9 lpm since area 2 (accumulator charge) in Figure 14 is equal to area 1 (accumulator discharge). Taking into account the time varying flow and pressure symmetry, two accumulators were selected and mounted on the manifold, see Figure 15(a).

Accounting for system losses, the average flow of 6.9 lpm is increased by 45% to 10 lpm (i.e. $10 \text{ cm}^3/\text{rev}$ at 1000 rpm). The selected hydraulic pump is of constant

pressure piston type, see Figure 15(b). The pump is driven by a three-phase, submersible induction motor, mounted externally to the dry bay for cooling purposes, and supplied through a star-delta starter.

Although in electrohydraulic servo systems usually servo valves are used, here proportional valves were employed, as they are more tolerant to contamination, and are less expensive. Eighteen 4-way, 3-position, closed center proportional, high-response valves without electrical position feedback were selected (model type:



Figure 13. A CD SX 32/22 DK 229 S type, double action cylinder (Conforti Oleodina-mica).

SP08-47CL). The valves are of the needle type, and can be all mounted on custom-made manifolds, reducing complexity, number of hoses, and undesired hydraulic dynamics. Figure 16 shows the flow–pressure drop valve curves $Q-\Delta p$ for various orifice openings and their frequency response in the form of a Bode diagram.

Figure 17 shows the resulting flow–pressure drops at the valve ($Q-\Delta p$ curves) for their mechanical load of each leg joint during the desired trajectory for legs 1, 2, 3.

The load $Q-\Delta p$ requirements must lie under the valve characteristic (valve curve) for some % opening. In all plots in Figure 17, a 40% open valve curve is displayed

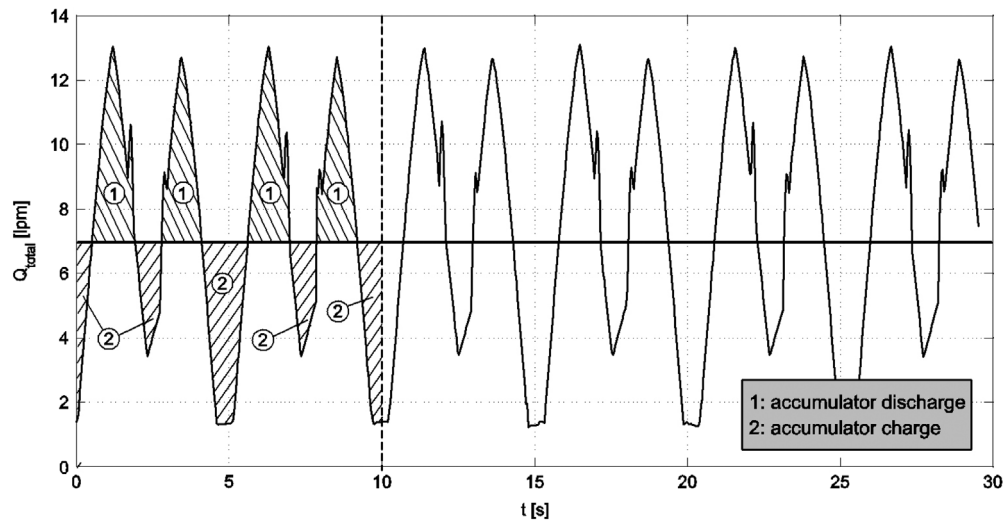


Figure 14. Diagram of the time varying flow and the accumulator contribution.

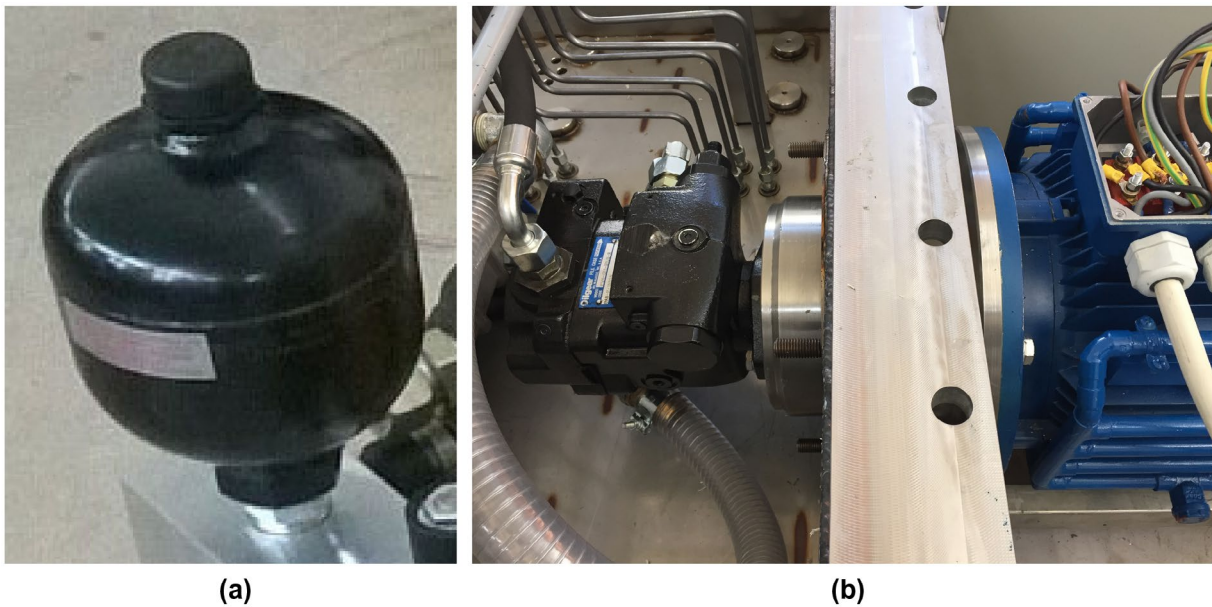


Figure 15. (a) One of the two HYDAC, SBO210 series, diaphragm-type accumulators, (b) the PVM Oilgear constant pressure, axial piston variable pump.

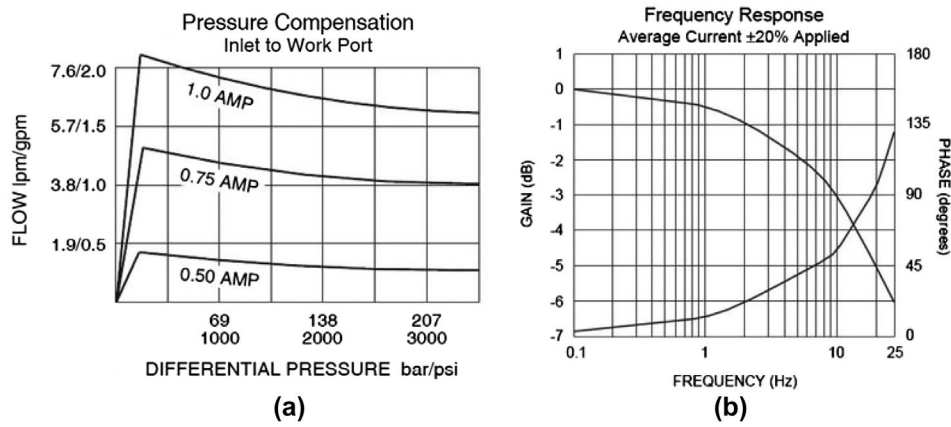


Figure 16. (a) The flow–pressure drop valve curves and (b) the frequency response of the proportional valve (type SP08-47CL, HydraForce).

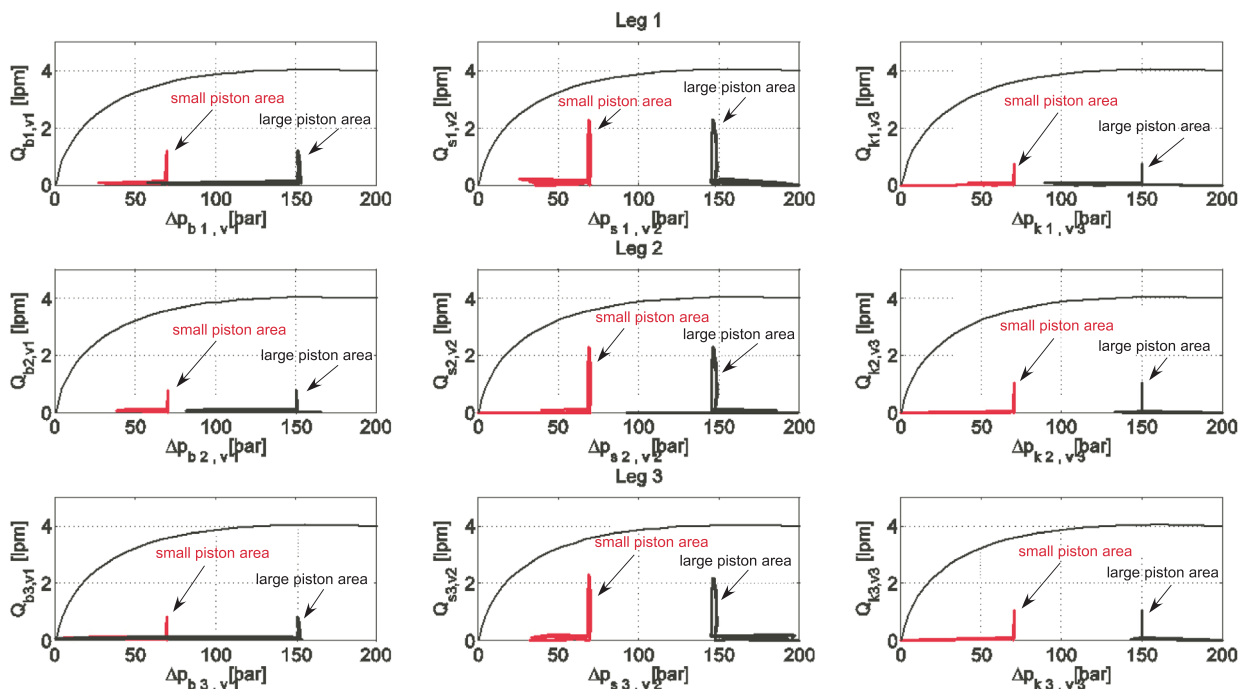


Figure 17. Load requirements in the flow–pressure drop valve diagram for the leg cylinders 1, 2, 3.

covering the two load curves that correspond to flow inputs (large piston area, i.e. main flow) and flow outputs (small piston area, i.e. return flow). The valve bandwidth of 25 Hz, see Figure 16(b), is adequate compared to the flow frequency requirements, about 2 Hz.

The design of the two custom-made valve manifolds supports nine needle valve connections and was chosen as it provides fewer potential leak points than conventional distribution manifolds. The two accumulators are also mounted on the two manifolds, increasing their responsiveness, see Figure 15(a). A hydraulic control valve (SP08-47CL) and one of the two manifolds are shown in Figure 18(a) and (b), respectively.

The hydraulic sub-circuit for the three cylinders of a single leg is depicted in Figure 19. The HexaTerra assembled hydraulic power unit is presented in Figure 20, while the main hydraulic system components are presented in Table 5.

4. Stability and control design

4.1. Maintaining stability

In generating joint angle commands, traditional locomotion algorithms do not take into account the inertial position and orientation of the hexapod main body and feet. The outcome is that the gait generation is calculated in a body-fixed coordinate system, not considering the

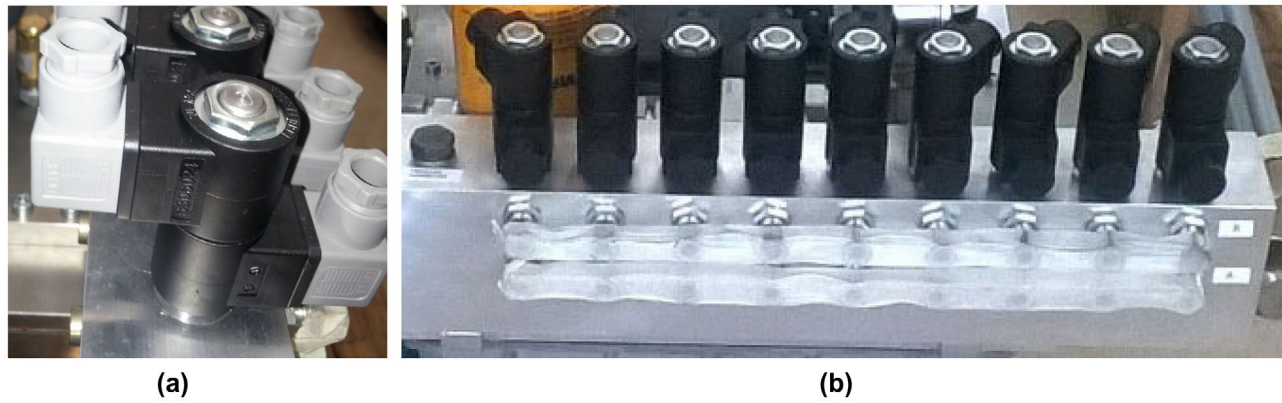


Figure 18. (a) The SP08-47CL valve, (b) one of the two custom-made manifolds.

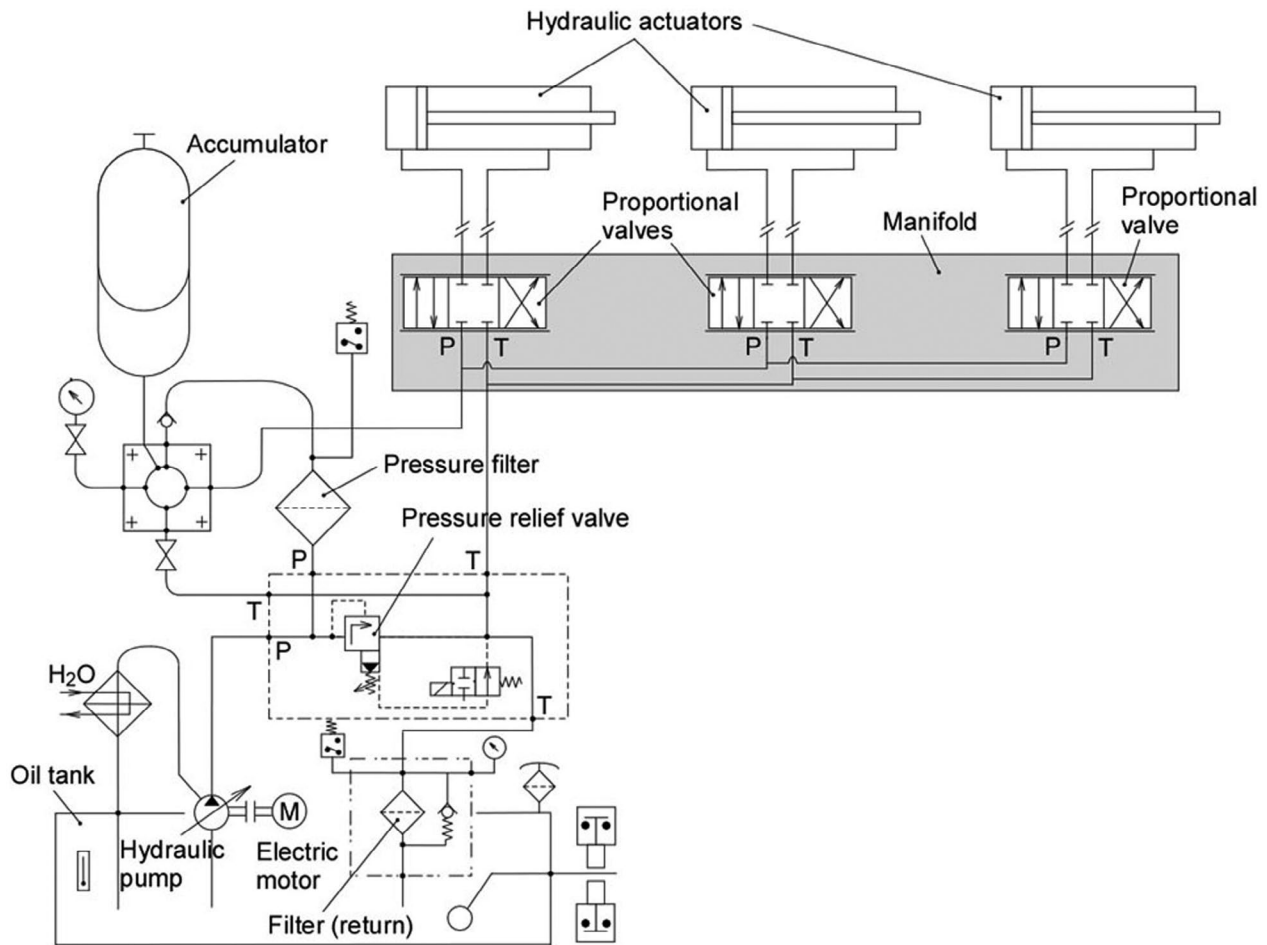


Figure 19. Hydraulic subcircuit for three cylinders of the HexaTerra servosystem.

stability of the system that is affected from the terrain variation. When the hexapod moves on a slope, these locomotion algorithms result in reduced static stability margin as shown in Figure 21. However, in the case of the underwater hexapod, subject to slopes and forces not found in dry environments, stability must be considered carefully.

An Inertial Locomotion Algorithm (ILA) is needed for maintaining predefined static stability margins during gaiting on uneven terrain [26]. The stability margin can be predicted regardless of the terrain and does not depend on the position at which the robot will end up when moving on unknown and uneven terrain. The algorithm relies on

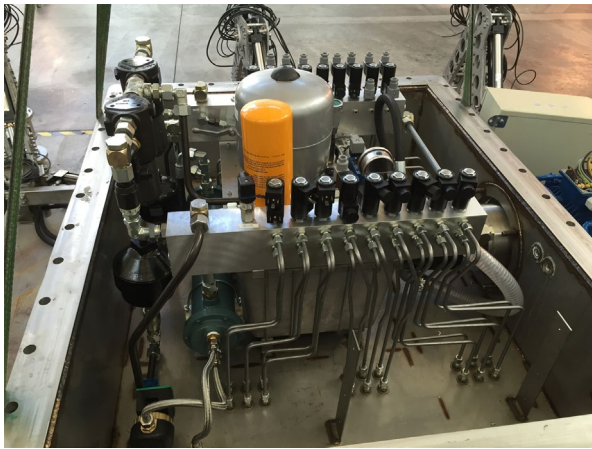


Figure 20. The assembled hydraulic power unit of the HexaTerra servosystem.

an IMU to obtain main body orientation, and on a planner commanding hexapod legs so that a predefined static stability margin is maintained. Since the static stability margin is not affected by the COM position along the Z axis as measured with respect to the Inertial Coordinate System (ICS), (inertial Z axis parallel to gravity), all motions of the main body COM and feet are initially planned on the horizontal plane (inertial XY). The desired vertical inertial coordinate Z of the main body COM is provided by the hexapod configuration obtained with feedback from the joint angles, modified by the Body Correction Algorithm (BCA), along with the main body roll and pitch angles. Since the ILA is initially implemented as if the terrain is flat (on the inertial XY plane), and the effect of the uneven terrain is then introduced (calculation of inertial Z axis for main body to ensure static stability margin is within desired range), this strategy allows a number of gaiting algorithms that are developed for flat and even terrain to be extended for rough terrain, including slopes and obstacles.

The ILA is outlined in detail in Figure 22. The current position and orientation of the hexapod body and feet with respect to the ICS, see Figure 23, are calculated in the beginning of each step using the known geometrical

characteristics of the hexapod and IMU and joint encoder measurements.

A Body-fixed Coordinate System (BCS) is placed at the center of mass with the BCS X axis parallel to the hexapod longitudinal axis, see Figure 23. The Z axis of the Body-fixed Coordinate system is opposite to the gravity vector when the hexapod is in neutral standing position.

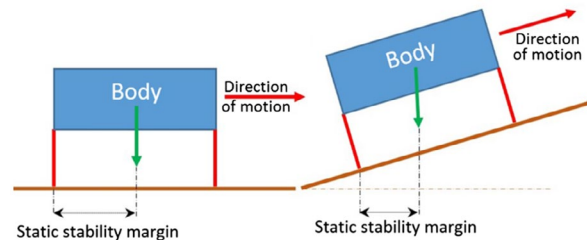


Figure 21. Static stability margin reduction when moving on a slope.

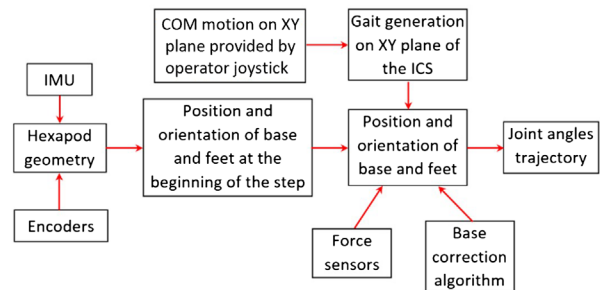


Figure 22. Robot Inertial Locomotion Algorithm (ILA).

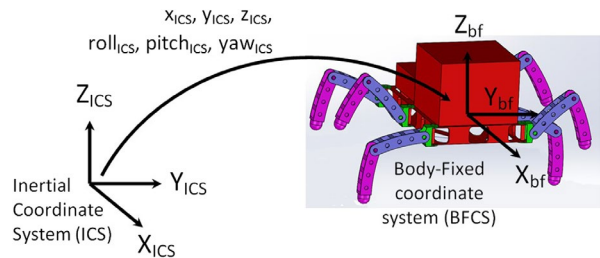


Figure 23. Inertial and Body-fixed Coordinate Systems.

Table 5. Main hydraulic components of the hydraulic system.

Component	#	Description
Cylinders	18	Diameters:32 mm /22 mm Lengths of base cylinder: 365 mm /272 mm, max. stroke 93 mm Lengths of shoulder cylinder: 632 mm /402 mm, max. stroke 230 mm Lengths of knee cylinder: 550 mm /362 mm, max. stroke 188 mm
Valves	18	Max. flow: 7.4 lpm, operating pressure: 240 bar
Pump	1	Constant pressure, axial piston variable pump, max. displacement: 10.8 cm ³ /rev, max. speed: 3600 rpm, max. pressure: 293.1 bar
Motor	1	Submersible, 6 pole, 3-phase, 400 V, nominal power: 4 kW, nominal speed: 1000 rpm
Star-Delta Starter	1	3-phase, 410 V, 50 Hz
Manifold Accumulators	2	Diaphragm type, 0.7 L, operating pressure 110 bar
Tank	1	40 L

For computational simplicity, the ICS is placed at the hexapod COM at the beginning of each step. The design of the hexapod locomotion for both the main body and the feet is initially made on the ICS XY plane by the controller so that the desired static stability margin can be predefined. The inertial Z coordinates for the feet after a step are determined by the ground reaction as obtained by the feet force sensors. During the implementation of a single step and when the foot is approaching the ground, the trajectory of the feet is parallel to the Z axis of the ICS, and when it touches the ground, it is commanded to stop. The foot design and the embedded force sensor allow gradual deceleration, providing smooth contact with the terrain. The desired Z (ICS) coordinate of the hexapod main body as well as its orientation (roll and pitch angles) are calculated in real time using the BCA. Knowing the inertial position and orientation of the main body and the feet inertial positions, and using inverse kinematics of the hexapod, the desired joint positions are calculated. The commands of the operator interact with the controller during the phase of the gait generation as in Figure 22. The operator using the joystick moves the COM of the hexapod main body within the ICS and the motion of the feet are determined to maintain static stability.

Since the gait generation is implemented at the ICS horizontal (XY) plane, the static stability of the system can be predefined and not affected by the terrain variation, slopes, or obstacles that the hexapod will step on during its motion as shown in Figure 24. Therefore, the static stability for horizontal and inclined motion is identical.

In the implementation of the BCA, the position and orientation of the main body are calculated. The BCS XY plane is compared to the support plane coordinate system, as in Figure 25 (defined by the supporting feet), and the errors of the two Euler angles (roll and pitch) as well as of the translation d along the Z axis are calculated according to

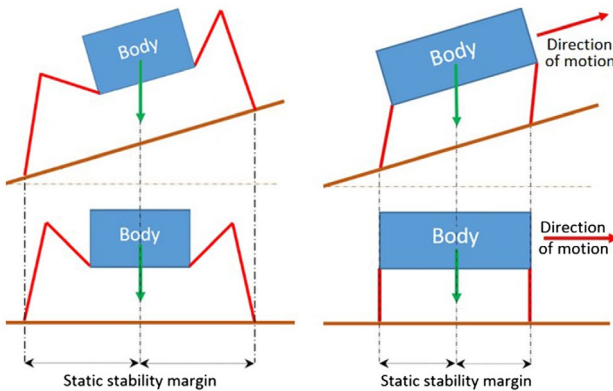


Figure 24. Static stability margin of the ILA when moving on slope.

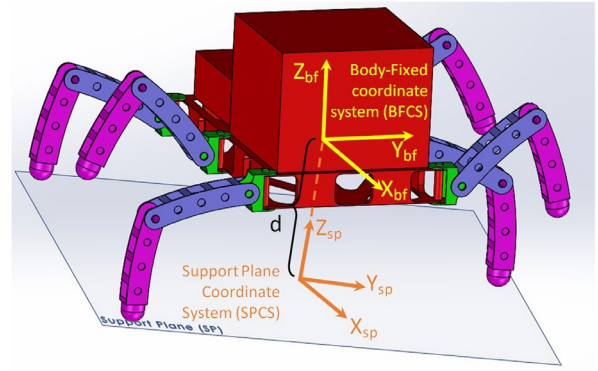


Figure 25. Definition of the Support Plane Coordinate System using the BFCs and an ADAMS model of the system.

$$\begin{aligned} \text{roll}_{err} &= \text{roll}_{flat} - \cos^{-1}(B) \\ \text{pitch}_{err} &= \text{pitch}_{flat} - \cos^{-1}(A) \\ d_{err} &= d_{flat} - C / \sqrt{(A^2 + B^2 + 1)} \end{aligned} \quad (22)$$

where d_{flat} , roll_{flat} , and pitch_{flat} are the theoretical walking height of the COM, roll and pitch main body Euler angles when moving on flat terrain, and A , B , and C are the parameters of the support plane representation

$$z(x, y) = Ax + By + C \quad (23)$$

calculated on the body-fixed coordinate system.

These transformations are fed to the controller to ensure that the main body is *parallel* to the support plane given by (23), and that the body COM follows the representation of Figure 24. The generation of the controller next desired position uses these errors to reduce them gradually so that the stability requirements are fulfilled. The performance of the ILA was validated in the experimental hexapod using the Force-Angle-Stability Measure (FASM) [27].

4.2. Joint-level control

In order for the joint angles to follow the desired trajectories \mathbf{q}_d , a simplified model-based control algorithm is implemented. This control scheme requires the dynamic model of the robot and estimates of the parameters involved, denoted by a $\hat{\cdot}$. Using this model, the torques $\boldsymbol{\tau}$ that must be applied are calculated according to

$$\begin{aligned} \mathbf{Q}_{ff} &= \hat{\mathbf{M}}(\mathbf{q}) \ddot{\mathbf{q}} + \hat{\mathbf{V}}(\mathbf{q}, \dot{\mathbf{q}}) + \hat{\mathbf{G}}(\mathbf{q}) + \hat{\mathbf{T}} \\ &= \mathbf{Q}_{ff} + \left(\mathbf{K}_v(\dot{\mathbf{q}}_d - \dot{\mathbf{q}}) + \mathbf{K}_p(\mathbf{q}_d - \mathbf{q}) \right) \end{aligned} \quad (24)$$

where \mathbf{K}_p , \mathbf{K}_v are diagonal positive definite control gain matrices added to undertake and correct possible errors and diversions.

The required angles of each DOF are calculated every 16 ms to fulfill the operator commands and the static stability as presented in Figure 24. To achieve this, the current support plane is calculated, and then the body Z, roll and pitch coordinates corrections (22) are obtained using the BCA. Using the inverse kinematics of the hexapod, the desired joint angles are calculated for the next step of the controller. Then, the dynamic model of the hexapod gives the joint torques, which correspond to the obtained trajectories and loads. The resulting forces, positions, and speeds of all DOFs are transformed into cylinder pressure, position, and flow using the geometry of the feet.

Using a simplified model for the hydraulic actuation, see Figure 26, we can calculate the required opening of the control valve, and using the manufacturer plot of valve performance, the control current to be sent to the proportional valve can be found.

To this end, we use Equation (6) for both valve orifices. We use two coefficients for the high- and low-pressure line of the valve, respectively, according to the manufacturer figures. Neglecting hose resistance, and using valve pressure drop equation and pressure compatibility, for the forward motion, the following equations are obtained

$$\begin{aligned} p_s &= p_{L,p_1} + K_{1f} Q_{L,p_1}^2 \\ p_{L,p_2} &= K_{2f} Q_{L,p_2}^2 \end{aligned} \quad (25)$$

Similarly for the backward motion, the following equations are obtained,

$$\begin{aligned} p_s &= p_{L,p_2} + K_{1b} Q_{L,p_2}^2 \\ p_{L,p_1} &= K_{2b} Q_{L,p_1}^2 \end{aligned} \quad (26)$$

where p_s is the supply pressure, p_{L,p_1} and p_{L,p_2} are the pressures at the two sides of the piston, Q_{L,p_1} and Q_{L,p_2} are the flows in the two lines, K_{1f} the valve pressure drop coefficient for the high-pressure line and forward motion, K_{2f} the valve pressure drop coefficient for the low-pressure line and forward motion, K_{1b} the valve pressure drop coefficient for the high-pressure line and backward motion, and K_{2b} the valve pressure drop coefficient for high-pressure line and backward motion. Based on manufacturer data, the following holds for these coefficients

$$\begin{aligned} K_{2f} &= K_{1f}/4.5 \\ K_{2b} &= K_{1b}/4.5 \end{aligned} \quad (27)$$

Using the following equations,

$$\begin{aligned} F &= p_{L,p_1} A_1 - p_{L,p_2} A_2 \\ u &= \frac{Q_{L,p_1}}{A_1} = \frac{Q_{L,p_2}}{A_2} \end{aligned} \quad (28)$$

where F is the applied force and u the piston speed, the coefficients K_{1f} and K_{1b} for forward and backward hydraulic cylinder motion are found to be:

$$K_{1f}^{-1} = \frac{u^2 A_1^2 \left(1 + \frac{(A_2/A_1)^3}{4.5}\right)}{\left(p_s - \frac{F}{A_1}\right)} K_{1b}^{-1} = \frac{u^2 A_2^2 \left(1 + \frac{(A_2/A_1)^3}{4.5}\right)}{\left(p_s + \frac{F}{A_2}\right)} \quad (29)$$

Using (29) and the characteristics provided by the valve manufacturer, the driving current that corresponds to the opening of the proportional valve is calculated, and sent to the valves.

4.3. Sensors

The implementation of the control algorithms requires measurement of all leg joint angles. To this end, high-resolution (13 bit), IP68, magnetic, absolute encoders were selected, see Figure 27(a).

Since the hexapod will operate in unknown terrains, force sensors are used on each toe, so that the control system knows where the ground is. The magnitude of the force is used also by the model-based controller to calculate a feedforward term for the joint-level control. The force sensors used are single-axis, IP68 load cells capable of measuring forces up to 18 kN, capacity that can protect from impact forces that may be applied during gaiting of the robot, see Figure 27(b). Each sensor is used in series with a spring, which provides input for the smooth approach of the toe on the seabed terrain.

Finally, for safety reasons, the humidity and temperature of the hexapod dry bay are monitored using two sensors. The first ensures that inside the bay, no liquefaction will take place due to difference in the temperatures

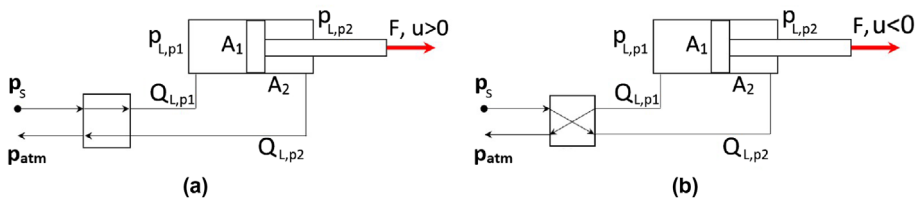


Figure 26. Simplified hydraulic circuit, (a) forward and (b) backward motion.

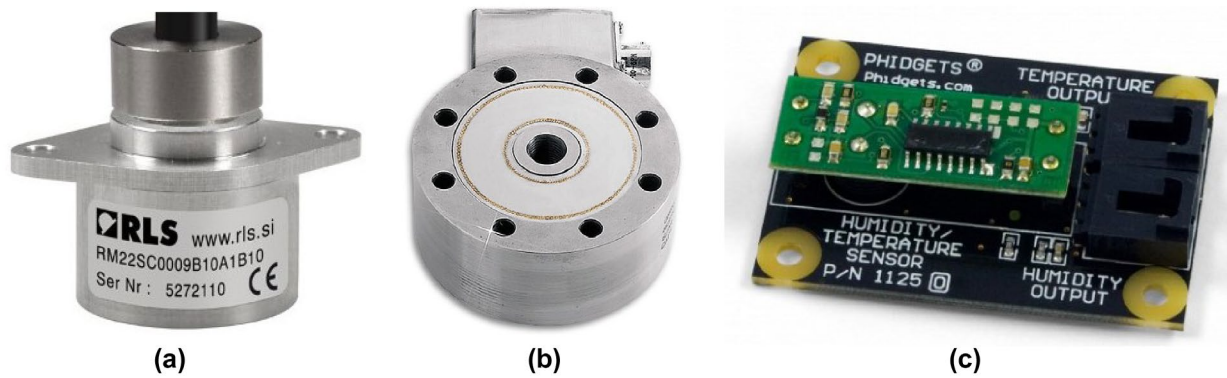


Figure 27. (a) Joint absolute encoders, (b) Omega IP68 load cell on hexapod toes, (c) Phidgets humidity/temperature sensor.

of the housing (cooled by the surrounding water) and the air within the bay. The second ensures that the electronics will operate within their operational temperature margin. A temperature/humidity sensor from Fidgets was used for this purpose, see Figure 27(c).

4.4. Control implementation

The implementation of the hexapod controller is realized using three 6-axis Galil controllers, a mini PC, and 18 valve controllers, all installed in the robot dry bay. Figure 28 shows how the control hardware is connected including the system sensors.

The mini PC uses an Intel Core i5-4250U processor and is responsible for the high-level control. It runs the software that implements the gait generation algorithms (inertial locomotion algorithm and BCA), the model-based controller, and the communication link with an external operator PC/GUI. It is also responsible for system safety, as it monitors the hydraulic pressure, the temperature, and the humidity of the hexapod dry bay housing the hydraulics and the electronics.

The three Galil controllers, see Figure 29(a), run the low-level control of the system, each of them responsible for two legs, i.e. coordinating 6 axes in total. These controllers run the PD loop, with the model-based term provided to them by the mini PC, once every 181 ms. To achieve tight synchronization of the axes, the inverse kinematics is solved within the Galil controllers, providing the quick response needed especially during the foot approach to the terrain. The desired positions for the degrees of freedom are calculated every 16 ms.

The HydraForce EVDR-0201A valve controllers convert the voltage commands that are generated by the Galil controllers to current that drives the proportional hydraulic valves, see Figure 29(b).

The output of the Galil controller is a $-10/+10$ V analog control signal that is calculated using the model-based controller feedforward and the PID for each of the DOFs. This signal needs to be transformed to an opening of the valve that results in cylinder motion. Due to the design of the proportional valves, the opening of the valve is a function on the pulling coil current. Therefore, the voltage control signal needs to be converted to a driving current

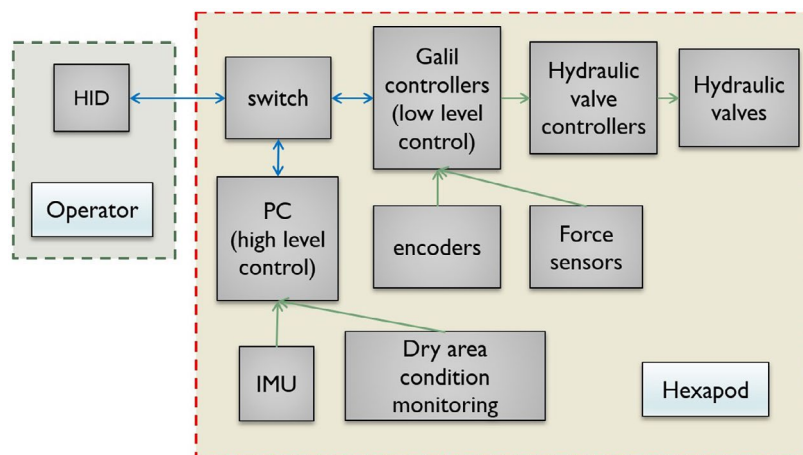


Figure 28. Control hardware schematic.

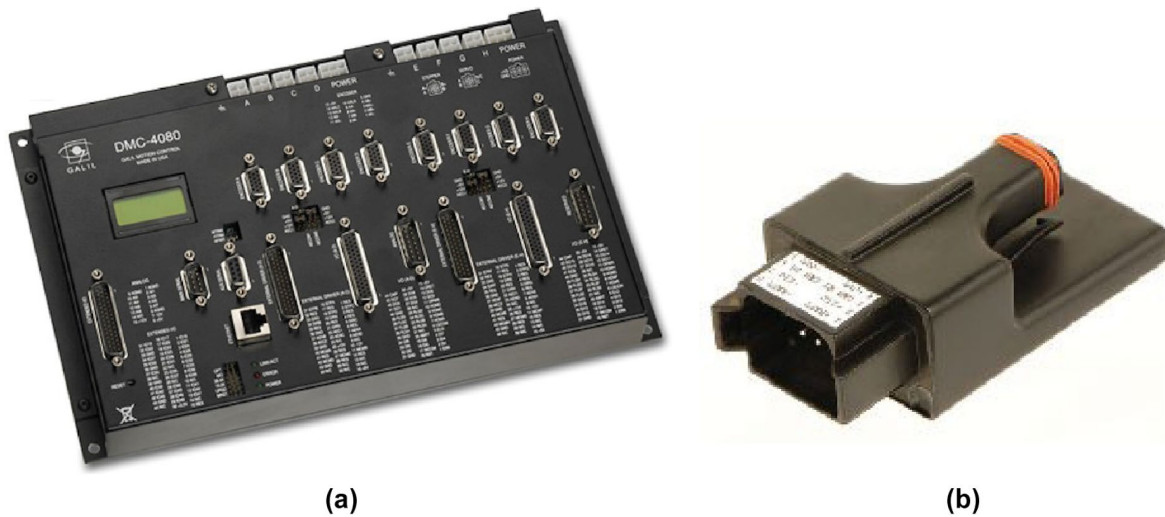


Figure 29. Low-level control hardware. (a) Galil DMC-4060, 6-axis motion controller, (b) the HydraForce EVDR-0201A valve controller.

for the valve coil. The valve controller implements this conversion with a configurable output according to the valve needs. Each proportional valve has a deadband, which is the minimum current that is required for the valve to open. Using the valve controller configuration, the dead band current is set to correspond to near zero voltage control command, therefore approximating a linear system behavior. The maximum current output of the controller is 2A.

5. Experimental results

The developed hexapod, shown in Figure 1, weighs in air 1200 kg. However, due to its dry bay, its submerged weight is only 250 kg, allowing the execution of high-speed tripod gaits, even on sloped terrain. As the hexapod is modeled in ADAMS, it was critical to match simulation results to dry experiments, validating the design both for dry and wet environments.

5.1. Single leg experiments

For the initial leg testing, a post was set to support the leg during motion, see Figure 30.

Using this assembly, all types of gaits and modes of operation were tested. In addition, the capability of the hydraulics to create the support force has been validated. The foot has been pushed against the ground and the maximum reaction force of 2.7 kN was measured using the force sensor mounted on the foot, indicating the prediction that the hydraulics can support a wave gait even in dry tests. During the underwater gait, the buoyancy of the robotic system dramatically reduces its weight, therefore tripod and ripple gaits are all possible. The forces

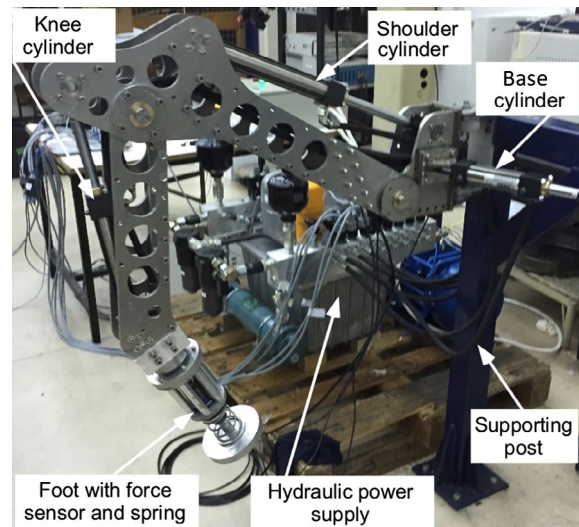


Figure 30. Single leg experiment setup. The leg is supported by the blue post and is driven by the hydraulic supply assembly next to it.



Figure 31. The hexapod performing a wave gait on the ground.

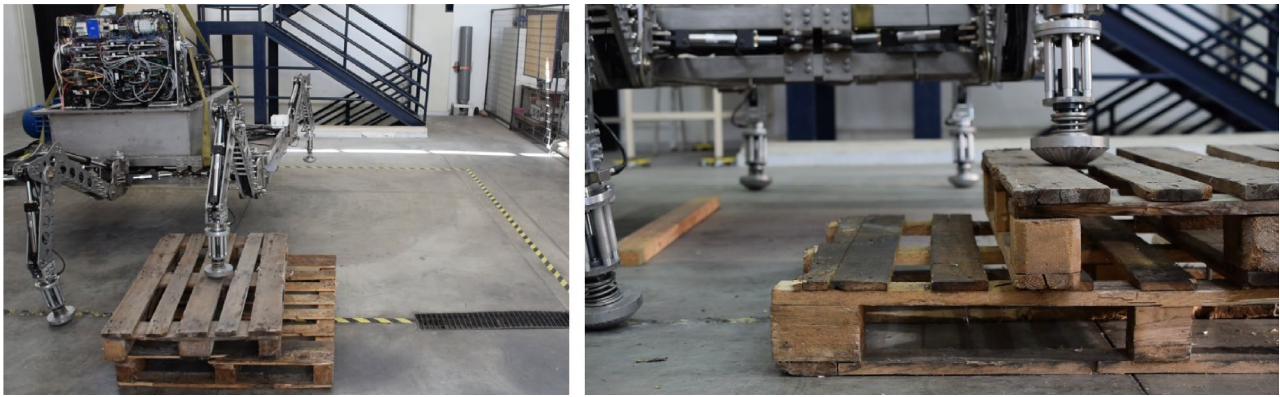


Figure 32. The hexapod overcoming a 150/300 mm obstacle.

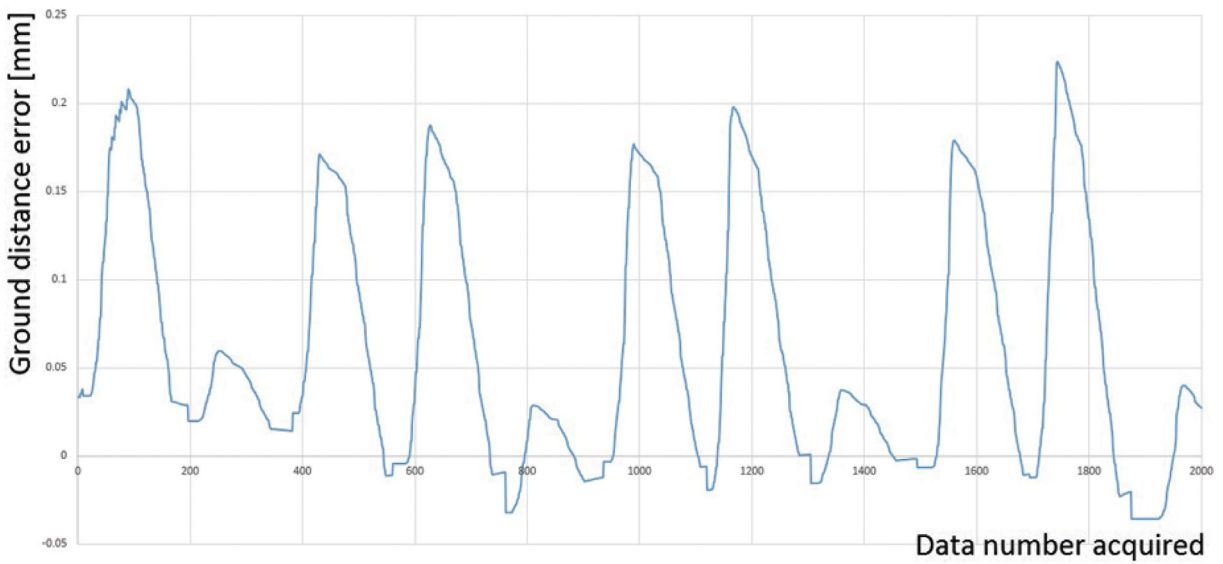


Figure 33. Main body height (ground distance) error obtained during testing.

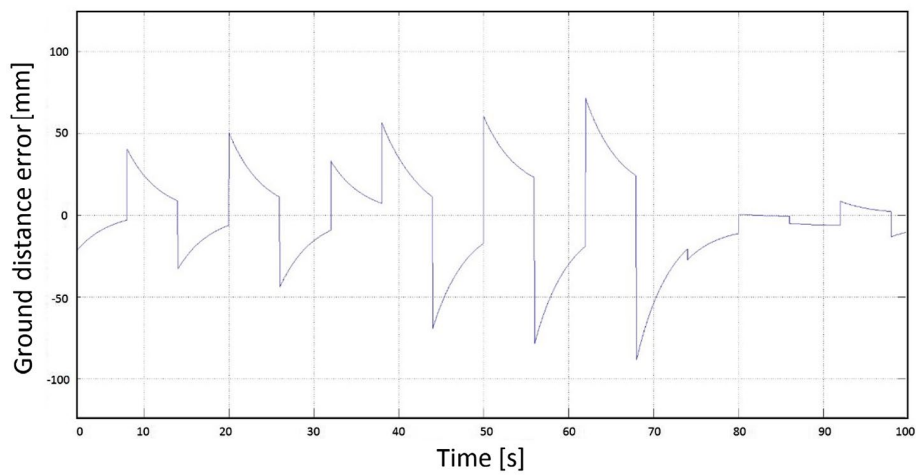


Figure 34. Main body height (ground distance) error obtained from simulation.

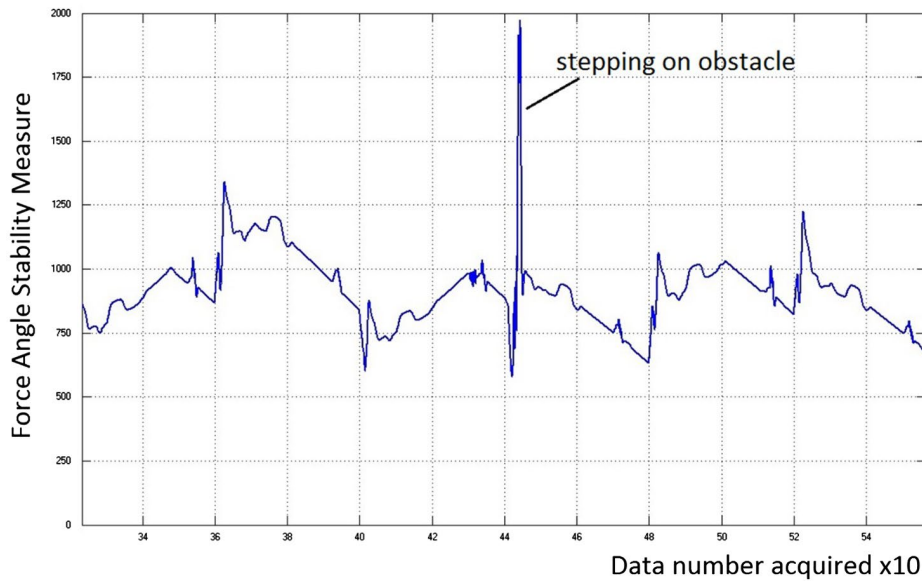


Figure 35. Force-Angle Stability Measure acquired during testing over obstacles.

measured at the foot were used to evaluate the simulation results for the torques applied at the leg joints.

5.2. Flat terrain performance

The hexapod was tested in dry tests using a wave gait, see Figure 31, and the results validated the theoretical design performance for the speed of the system that corresponds to the sizing of the hydraulic actuation.

The operator can choose between three operation modes for the movement of the robot: (a) *Drive mode*, where the robot moves forward/backward and turns with respect to the vertical, (b) *Crab drive mode*, where the orientation of the main body remains constant, and the robot can move forward/backward, left/right or diagonal using combination of the two, and (c) *Neutral mode*, where it can adjust the position and orientation of the main body in all 6 axes with all legs touching the ground. Forward, sideways, and diagonal motions were performed achieving dry speed of 15 mm/s. Full on the spot turning was successfully performed in 500s. During walking, the operator can adjust the stepping distance from the main body of the hexapod, as well as the height of the main body with respect to the ground.

5.3. Climbing performance

The hexapod was tested against single and combined objects and successfully overcame 150 mm/300 mm obstacles as shown in Figure 32. During the obstacle overcoming tests, the main body height error (body correction), as well as the FASM was monitored.

During the tests, the main body height error, i.e. commanded height minus the actual one, was measured. As shown in Figure 33, each time a leg steps over an obstacle, the error increases drastically, as the main body moves upwards. However, despite the discontinuous changes to the ground, i.e. from 0 to 150, and to 300 mm, this error is reduced rapidly due to the BCA. The observed behavior matches simulation results and theoretical expectations, and is displayed in Figure 34.

During the experiments, the FASM was monitored, too. Since the FASM is affected by the distribution of forces, when the hexapod steps on an obstacle a spike occurs. However, as can be seen in Figure 35, after stepping on an obstacle, the FASM maintains a high value, indicating that the BCA maintains stability regardless of stepping on the obstacle.

6. Conclusion

The design, development, and control for an 18 DOF electrohydraulic subsea hexapod robot were presented. The HexaTerra hexapod is designed for trenching and exploration tasks, able to overcome obstacles, slopes, drag, and currents. The leg design was obtained using optimization techniques. A dynamic model of the hexapod was developed using a Lagrangian approach, incorporating a ground model for estimating ground reactions. The electrohydraulic design was based on a worst-case scenario and was implemented with a constant pressure supply driving proportional valves, mounted on a custom manifold design. The components were selected taking into account the leg kinematics and system dynamics, resulting in minimum size, and cost.

The algorithms implemented on the robot control system were presented. Using feedback from the 18 encoders, the toe force sensors, and an IMU, the Inertial Locomotion Algorithm maintains static stability regardless of the variation of the terrain. The gaiting algorithms were designed with respect to an inertial coordinate system rather than to a body-fixed traditionally used in hexapod gait design. The Body Correction Algorithm adjusts the position and orientation of the main body to achieve the desired stability. Each joint is controlled by a model-based feedforward PD-type controller computed using the dynamics and the hydraulic actuation models. The controller was implemented on a mini PC, and on three 6-axes Galil controllers, driving the joint proportional valve controllers.

The robot was successfully tested in dry conditions using a wave gait. All modes of operation were tested, and the robot was able to overcome a combined obstacle of 150/300 mm height. Experimental results of the response of the BCA and the FASM indicate the effectiveness of the developed electrohydraulic actuation system.

Note

1. Overhead is the length of cylinder from joint to joint when zero stroke is selected. For instance, the overhead of a 32-mm piston diameter for a standard hydraulic cylinder (Conforti Oloedinamica SRL, ISO MP5 mounting) is 0.173 m.

Disclosure statement

No potential conflict of interest was reported by the authors.

Funding

This work was supported by the European Commission under the collaborative framework program funding scheme (Seventh Framework Programme) [FP7-SME-2008-2 – Grant agreement n° 605420].

Notes on contributors

Ioannis Davliakos received his diploma from the Aristotle University of Thessaloniki (AUTH), in 1998, in Mechanical Engineering (ME). He received his MS degree and PhD degree from the National Technical University of Athens (NTUA) in 1999, and 2007, respectively, all in ME. Currently, he is laboratory teaching staff and a research associate in the ME Department of NTUA, co-teaching Circuits and Systems, Electromechanical Systems, and Robotics. He is a member of the Technical Chamber of Greece, and the Hellenic Association of Mechanical and Electrical Engineers. His research interests are in Robotics, Dynamic Systems and Control, Electrohydraulic Servo Control, and Exoskeletons.

Ioannis Roditis received his diploma in Mechanical Engineering and MSc in Automatic Control Systems from the

National Technical University of Athens in 2006 and 2008, respectively. He joined Innora S A in 2009, where he works as a mechanical designer and automation engineer until now. His research interests include robotics, mechanical design, dynamic modeling, and industrial automation. He is a member of the Technical Chamber of Greece.

Klajd Lika received a diploma in Mechanical Engineering (ME) from the National Technical University of Athens (NTUA), in 2013, and subsequently until 2016, he was a research assistant with the Control Systems Laboratory of ME of NTUA. In 2016, he joined the Robotics Systems Laboratory of ETH Zurich, where currently he is a scientific assistant. His research interests lie in the design of optimized complex robotic systems, as well as of high-performance mechatronic devices for robotic systems. He holds an interest into converting high-end technology research into real-life applications/products.

Christina-Marina Breki holds a diploma in Informatics and Telecommunications from the National and Kapodistrian University of Athens (UoA). Her thesis involved research at the National Center of Scientific Research ‘Demokritos’, on the fractal and multifractal analysis of PET/CT images. Her work has been published in the European Journal of Nuclear Medicine and Molecular Imaging (EJNMMI). She joined Innora in 2015 and worked on the development of applications for robotics. Currently she pursues a master’s degree in Control and Computing at the UoA.

Evangelos Papadopoulos received a diploma in Mechanical Engineering from the National Technical University of Athens, (NTUA), Greece, in 1981, and subsequently a MS (1983) and a PhD degree (1991) in Mechanical Engineering from the Massachusetts Institute of Technology (MIT). In 1991, he was appointed a lecturer at MIT and subsequently he joined McGill University, Montreal, Canada as an assistant professor. He joined the NTUA in 1997, where he is currently a professor of Mechanical Engineering. He teaches courses in Robotics, Controls, Mechatronics, Circuits and Systems, and Electromechanical Systems. Papadopoulos is a fellow of the ASME, an associate fellow of the AIAA, and a senior member of the IEEE. He serves as an associate editor of the Mechanism and Machine Theory, of the ASME Journal of Dynamic Systems, Measurement and Control, of the IEEE Robotics and Automation Letters, and of the Frontiers in Space Robotics. He conducts research in the areas of robotics including space robotics, biomimetic and legged robots, microrobotics, mechatronics, haptic devices, simulators, design, and applied control, with funding from national, European, Canadian, and industrial sources. He is author or co-author of more than 250 technical papers, and of three books in Greek.

References

- [1] Jelali M, Kroll A. Hydraulic servo-systems. modelling, identification and control. London: Springer; 2003.
- [2] Merritt HE. Hydraulic control systems. New York (NY): J. Wiley & Sons; 1967.
- [3] Nonami K, Barai, RK Irawan A, et al. Hydraulic actuated hexapod robots. Design, implementation and control. Japan: Springer; 2014.
- [4] Raibert M. Legged robots that balance. Cambridge (MA): MIT Press; 1986.

- [5] Boston Dynamics. LS3 – Legged squad support systems. 2013; Available from: http://www.bostondynamics.com/robot_ls3.html.
- [6] Raibert M, Blankespoor K, Nelson G, et al. BigDog, the rough-terrain quadruped robot. Proceedings of the 17th IFAC World Congress; Seoul, Korea; 2008 Jul.
- [7] Li Y, Li B, Ruan J, et al. Research of mammal bionic quadruped robots: a review. In: IEEE 5th International Conference on Robotics, Automation and Mechatronics (RAM); 2011 Sept 17–19; Qingdao, China. p. 166–171.
- [8] Semini C, Tsagarakis NG, Vanderborght B, et al. HyQ – hydraulically actuated quadruped robot: hopping leg prototype. In: 2008 2nd IEEE RAS & EMBS International Conference on Biomedical Robotics and Biomechanics; Scottsdale, Arizona, USA; 2008. p. 593–599.
- [9] Semini C, Barasuol V, Goldsmith J, et al. Design of the hydraulically actuated, torque-controlled quadruped robot HyQ2Max. IEEE/ASME Tr Mechatron. 2017;22(2):635–646.
- [10] Bjelonic, M, Homberger T, Kottege N, et al. Autonomous navigation of hexapod robots with vision-based controller adaptation. In: 2017 IEEE International Conference on Robotics and Automation (ICRA); Singapore; 2017. p. 5561–5568.
- [11] Roennau, A, Heppner G, Nowicki M, et al. Lauronv: a versatile six-legged walking robot with advanced maneuverability. In: 2014 IEEE/ASME International Conference on Advanced Intelligent Mechatronics; Besancon, France; 2014 Jul; p. 82–87.
- [12] Hyon S-H, Yoneda T, Suewaka D. Lightweight hydraulic leg to explore agile legged locomotion. In: 2013 IEEE/RSJ International Conference on Intelligent Robots and Systems (IROS); 2013 Nov 3–7; Tokyo, Japan; p. 4655–4660.
- [13] Ma M, Wang J, Hydraulic-actuated quadruped robot mechanism design optimization based on particle swarm optimization algorithm. In: 2nd Int. Conference on Artificial Intelligence Management Science and Electronic Commerce (AIMSEC); Deng Feng, China; 2011 Aug; p. 4026–4029.
- [14] Rong X, Li Y, Meng J, et al. Design for several hydraulic parameters of a quadruped robot. Int J Appl Math Inf Sci. 2014;8(5):2465–2470.
- [15] Rong X, Li Y, Ruan J, et al. Design and simulation for a hydraulic actuated quadruped robot. J Mech Sci Tech. 2012;26(4):1171–1177.
- [16] J. Deere Co., Finland. 1995. Available from: <http://www.theoldrobots.com/Walking-Robot2.html>
- [17] Barai RK, Nonami, K. Locomotion control of a hydraulically actuated hexapod robot by robust adaptive fuzzy control with self-tuned adaptation gain and dead zone fuzzy pre-compensation. J Intell Rob Syst. 2008 Sept;53:35–56.
- [18] Kekäläinen T, Mattila J, Virvalo T. Development and design optimization of water hydraulic manipulator for ITER. Fusion Eng Des. 2009;84:1010–1014.
- [19] Akizono J, Iwasaki M, Nemoto T, et al. Field test of aquatic walking robot for underwater inspection. In: Mechatronic System Engineering. Vol. 1, Dordrecht, Netherlands: Kluwer Academic Publishers; 1990, p. 233–239.
- [20] Bong-Huan J, Hyungwon S, Banghyun K, et al. First field-test of seabed walking robot CR200. 2013 OCEANS – MTS/IEEE San Diego; 2013 Sept.
- [21] Available from: http://cordis.europa.eu/project/rcn/109873_en.html
- [22] Aggelopoulou E, Rekleitis G, and Papadopoulos E. Optimal leg-sequence selection for an underwater hexapod robot in the presence of slopes and external forces. In: 25th Mediterranean Conference on Control and Automation (MED); Valletta, Malta; 2017 Jul. p. 340–345.
- [23] Blackburn JF, Reethof G, Shearer JL. Fluid power control. Cambridge (MA): MIT Press; 1960.
- [24] Thayer WJ. Specification standards for electrohydraulic flow control servovalves. Tech Bull, 117, 1962; Aurora (NY): Moog Inc. Control Div., E.
- [25] Papadopoulos E, Gonthier Y 2002. On the development of a real-time simulator engine for a hydraulic forestry machine. Int J Fluid Power. 3(1): 55–65.
- [26] Roditis I, Nitsos T, Porichis A, et al, Maintaining static stability and continuous motion in rough terrain hexapod locomotion without terrain mapping. In: 24th Mediterranean Conference on Control and Automation (MED); Athens; 2016 Jun. p. 545–550.
- [27] Papadopoulos EG, Rey DA. A new measure of tipover stability margin for mobile manipulators. In: Proceedings of IEEE International Conference on Robotics and Automation; Vol. 4. Minneapolis (MN); 1996 Apr. p. 3111–3116.